

Contents lists available at ScienceDirect

# Energy

journal homepage: www.elsevier.com/locate/energy





# Comparative study on supercritical carbon dioxide cycle using air-cooler and water-cooler

Yaqin Liu<sup>a</sup>, Jinliang Xu<sup>a,b,\*</sup>, Tianze Wang<sup>a</sup>

- a Beijing Key Laboratory of Multiphase Flow and Heat Transfer for Low Grade Energy Utilization, North China Electric Power University, Beijing, 100026, China
- b Key Laboratory of Power Station Energy Transfer Conversion and System (North China Electric Power University), Ministry of Education, Beijing, 102206, China

#### ARTICLE INFO

Keywords: sCO<sub>2</sub> cycle Air-cooler Water-cooler Pressure drop Heat transfer Cost

#### ABSTRACT

Supercritical carbon dioxide (sCO<sub>2</sub>) cycle has high efficiency and fast response as load changes. It is important to examine whether the sCO<sub>2</sub> cycle is suitable in arid area. Hence, we explore the effect of air-cooler and water-cooler on the performance of a 300 MW sCO<sub>2</sub> coal fired generation system. Flow and heat transfer models were established for air-cooler and water-cooler. The later includes shell-tube-heat-exchangers and a cooling tower. We show a 0.8 % efficiency drop using air-cooler instead of water-cooler, at an air temperature of  $T_a = 20$  °C, which increases as  $T_a$  rises. The increased temperature of sCO<sub>2</sub> and exergy destruction in air-cooler explain the efficiency penalty. Compared with cooling conditions for water-steam Rankine cycle, larger temperature difference exists in ~30 K level between sCO<sub>2</sub> and cooling fluids, explaining weaker efficiency penalty for sCO<sub>2</sub> cycle. Besides, the usage of air-cooler creates a 3.66 million RMB cost reduction than water-cooler. The raised on this study, the air-cooler induces mini efficiency drop and reduced cost, it is concluded that for sCO<sub>2</sub> cycle it is preferable to use the air-cooler, which is benefit to save the water resource in arid area.

# 1. Introduction

Carbon dioxide emission should be reduced to achieve the goal of carbon peak and carbon neutrality. Large scale utilization of renewable energies including solar energy and wind energy is necessary [1]. These renewable energies strongly rely on weather conditions, displaying periodic and oscillating characteristics [2], under which the coal-fired power generation system is changing the role from basic load supply to adjustable energy source, balancing unstable renewable energies [3, 4].

Supercritical carbon dioxide (sCO<sub>2</sub>) cycle uses  $CO_2$  to convert thermal energy into power. Compared with the water-steam Rankine cycle, the sCO<sub>2</sub> cycle easily reaches supercritical condition due to its lower critical parameters of 304.13 K/7.377 MPa [5]. Besides, the inlet vapor temperature entering turbines can be further increased to improve the system efficiency, due to more inert feature of  $CO_2$  with metallic surfaces than water-steam [6]. The faster response to load variations of sCO<sub>2</sub> cycle is attractive for coal-fired power generation to balance unstable renewable energies [7–9]. For the water-steam Rankine cycle, the load changing rate reaches 1–4 % Pe/min maximally [10,11], but for the  $CO_2$ 

power cycle, it may reach 6.35–10 % Pe/min [12–14].

Challenges of the sCO<sub>2</sub> cycle can be found in various review articles [15,16-18]. The progress includes the cycle analysis and the optimization [19-21], the component development [22-27], and the demonstration of power systems [28]. In China, the current author has leaded the investigation project on large scale sCO<sub>2</sub> coal-fired power generation system in the past five years [29-32]. Major progress is summarized here: (1) The overlap energy utilization is proposed to extract flue gas energy over entire temperature range [29]. (2) The modular boiler is proposed to overcome the challenging issue of ultra-large pressure drop induced efficiency penalty [30]. (3) The general heat transfer correlation of sCO<sub>2</sub> is developed to accurately predict the wall temperatures for key heat exchanger components [31]. (4) Other progresses include the construction of a convective heat transfer loop with pressures reaching 25 MPa and temperatures reaching 280 °C, maximally [32], a 300 KW test loop of sCO<sub>2</sub> boiler [33], and the investigations of sCO<sub>2</sub> turbines [34]. A 5 MW sCO<sub>2</sub> power plant driven by nature gas boiler has been successfully demonstrated and tested [35].

It is known that for thermal-power-conversion, cooler is a key component to dissipate the extra heat of power cycle to environment,

E-mail address: xjl@ncepu.edu.cn (J. Xu).

<sup>\*</sup> Corresponding author. Beijing Key Laboratory of Multiphase Flow and Heat Transfer for Low Grade Energy Utilization, North China Electric Power University, Beijing, 100026, China.

affecting the steady system performance and the transient characteristic of power plants [36]. Two types of coolers are used: water-cooler (WC) and air-cooler (AC) [37]. The former uses water to cool the cycle fluid of water-steam or CO2, with the water carried heat finally dissipated to environment in a water-cooling-tower (WCT) using the air-water mass transfer effect [37]. The latter uses air directly to cool the cycle fluid of water-steam or CO<sub>2</sub> [37]. Regarding the sCO<sub>2</sub> coal-fired power plants, available studies focus on the water-cooling by simply assuming an inlet water temperature such as 20 °C entering the cooler [30]. We note that some authors have performed the analysis of the cycle and the air-cooler performance for sCO2 cycle using solar energy as the heat source and air-cooler to dissipate extra heat to the environment [38-42]. The direct comparison between air-cooler and water-cooler are not involved in these references [40-42]. Besides, the comparative cost analysis between the air-cooler and water-cooler was not performed previously [38–42]. The original contribution of the present paper lies in the direct comparison between the two kinds of coolers as well as the costs analysis. The outcomes of the present paper provide the guideline for the engineering application.

Y. Liu et al.

Here, a short review is given on the cooling technologies for the water-steam Rankine cycle. Generally, the condenser keeps a constant saturation vapor temperature in the hotter fluid side, but keeps varied temperatures along the flow length in the cooling fluid side (water or air). Due to poorer heat transfer of air, the air-cooler elevates the vapor temperature and the corresponding pressure in the condenser, deteriorating the system performance [43,44]. The investigations conclude large efficiency penalty by using air-cooler instead of water-cooler [45]. For 50 MW water-steam Rankine cycle, the cycle efficiency decreases from 34.2 % to 32 % when an air-cooling-tower instead of a WCT is used. To decrease the efficiency penalty, various techniques have been applied, including enhanced heat transfer by using finned tubes [37,46,47], optimization of air flow field and air-fan operation [48–50].

Heat transfer in the cooler of sCO2 cycle differs from that of watersteam Rankine cycle. First, the cooler keeps varied temperatures across both the  ${\rm CO}_2$  fluid side and the cooling fluid side, influencing the roadmap and the pinch temperature location as well as the magnitude for the extra heat dissipation. Second, in the cooler, the CO<sub>2</sub> pressure may be ~7.6 MPa before entering the compressor, and the inlet CO2 temperature of the cooler can be  $\sim$ 90 °C [29], obviously higher than the water-steam temperature in the cooler for the Rankine cycle. In other words, the temperature difference of the cooler across the two sides of fluids for the sCO<sub>2</sub> cycle is larger than that for the water-steam Rankine cycle. This feature may decrease the sensitivity of the variation of the system performance with respect to the air-cooling and the water-cooling. Here, we perform a comparative study on the cooling technologies for large scale sCO2 coal fired power plants. We note that few articles deal with the air-cooler for solar energy driven sCO2 cycle, focusing on small scale system such as 25 MW power capacities [38-40,

In summary, previous studies on  $sCO_2$  cycle focus on the simple assumption of the cooling condition to dissipate extra heat of the system to environment [28–30], little is known whether the  $sCO_2$  cycle is suitable to operate in arid area where the water resource is scarce. One may ask questions such that what is the efficiency penalty when using air-cooler instead of water-cooler? What is the difference of the costs between the two coolers? The objective of this paper is to answer the above questions. In order to do so, flow and heat transfer models are parallelly described for the air-cooler and the water-cooler in section 2, considering the practical engineering designs. These correlations are

coupled with the cycle analysis. Major findings are described in section 3. Conclusions are summarized in section 4.

## 2. The numerical model

We start from the description of the  $sCO_2$  coal fired power plant in section 2.1. Then, the water-cooler and the air-cooler are described in section 2.2 and section 2.3, respectively. The coupling simulation of the cycle and the cooler is described in section 2.4.

# 2.1. The sCO<sub>2</sub> coal fired power plant

In this paper, a 300 MW power plant is investigated, which is suitable to provide flexible electricity output. The cycle integrates various components of the sCO<sub>2</sub> boiler (see Fig. 1). Different from solar energy and nuclear energy utilizations, flue gas energies of the sCO2 boiler should be extracted by the cycle over the entire temperature range. The overlap energy utilization is applied [29], consisting of a top-cycle responsible for high temperature flue gas energy absorption, and a bottom-cycle responsible for medium temperature flue gas energy absorption. Even though flow rates in the two cycles are different, thermodynamics parameters such as pressures and temperatures are similar for the two cycles. Therefore, the two cycles are merged into a single one to simplify the system configuration (see Fig. 1). The sCO2 boiler includes Heater 1, Heater 2, Heater 4a, Heater 4b, an air-preheater and an external-air-preheater (EAP). Compressors C1 and C2 provide the pressure heads to circulate the sCO2 flow. The high-pressure turbine T1 and low-pressure turbine T2 convert thermal energy into power. The high-temperature recuperator HTR1 and HTR2, as well as the low-temperature recuperator LTR account for internal heat recovery. To decrease the ultra-large flow rate induced pressure drop penalty, the modular boiler design is applied to yield the partial flow strategy [52].

In order to explore the effect of different coolers on the cycle performance, the extra heat of the system is dissipated to environment either by a water-cooler including a shell-tube-heat-exchanger and a WCT, or by an air-cooler (see Fig. 1). Table 1 lists the major design parameters for the 300 MWe power plant. Calculations of the cycle and the boiler are based on Ref. [30]. The net power  $W_{\rm net}$  and the cycle efficiency  $\eta_{\rm th}$  are

$$W_{\text{net}} = W_{\text{T1}} + W_{\text{T2}} - W_{\text{C1}} - W_{\text{C2}} \tag{1}$$

$$\eta_{\rm th} = \frac{W_{\rm net}}{Q_{\rm boiler}},\tag{2}$$

where  $W_{T1}$  and  $W_{T2}$  are the generated power by T1 and T2, respectively.  $W_{C1}$  and  $W_{C2}$  are the consumed power by C1 and C2, respectively,  $Q_{boiler}$  is the heat produced by the boiler. The cycle efficiency is strongly affected by the average heat absorption temperature  $T_{ave,ab}$  (heat source side), and the average heat release temperature  $T_{ave,re}$  (heat sink side) [53,54].

$$T_{\text{ave,ab}} = \frac{\sum Q_{\text{h}}}{\sum \Delta S_{\text{h}}} = \frac{\sum m(i_{\text{h,o}} - i_{\text{h,i}})}{\sum m\Delta s_{\text{h}}}$$
(3)

$$T_{\text{ave,re}} = \frac{\sum Q_{\text{c}}}{\sum \Delta S_{\text{c}}} = \frac{\sum m(i_{\text{c,o}} - i_{\text{c,i}})}{\sum m\Delta s_{\text{c}}},$$
(4)

where  $Q_h$  and  $Q_c$  are the heat absorbed in the heating process and that released in the cooling process, m is the mass flow rate in the heating

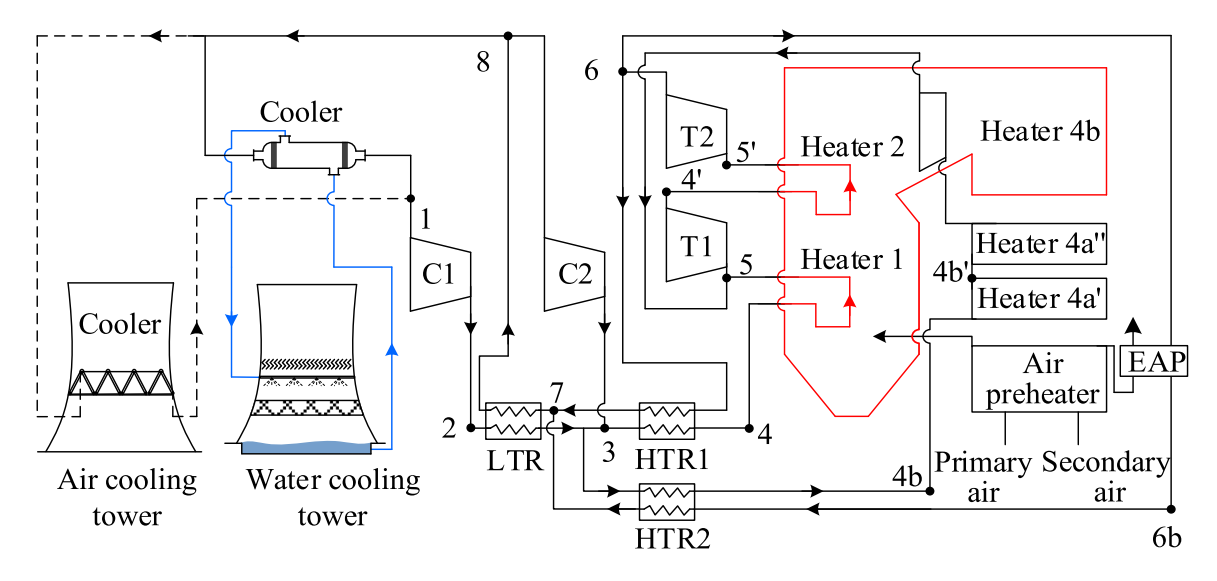


Fig. 1. sCO<sub>2</sub> coal fired power cycle coupling with the air-cooler or the water-cooler.

**Table 1** Design parameters of 300 MW sCO<sub>2</sub> power generation system [30].

parameters	values
net power, $W_{\text{net}}$	300 MW
inlet temperature of the turbine, $T_5$	620 °C
inlet pressure of the turbine, $P_5$	30 MPa
outlet temperature of $sCO_2$ in the hot side of high-temperature recuperator, $T_{4b}$	382 °C
inlet temperature of compressor C1, $T_1$	33 °C
inlet pressure of the compressor C1, $P_1$	7.6 MPa
isentropic efficiency of the turbine, $\eta_{T,s}$	0.90
isentropic efficiency of the compressor, $\eta_{C,s}$	0.93
pinch temperature difference in the recuperator, $\Delta T_{\rm R}$	10 °C
ambient temperature, $T_a$	20.0 °C

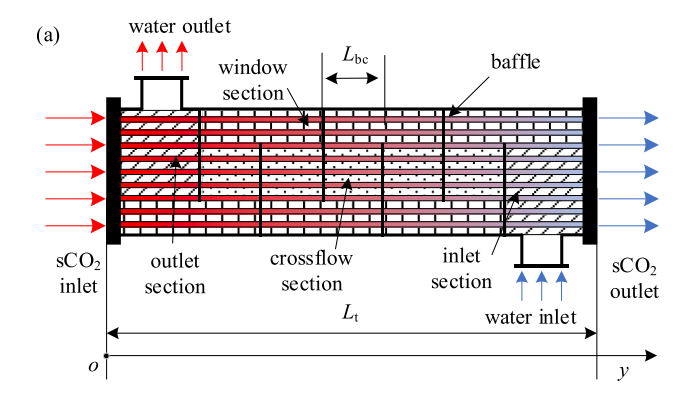
process, i and s are the enthalpy and entropy per unit mass. The subscript h and c mean the heating process and the cooling process, the subscript i and o mean the inlet and outlet, respectively.

#### 2.2. Water cooler

The water-cooler consists of a shell-tube-heat-exchanger (STHE) and a WCT. The cooling water and the  $sCO_2$  are flowing in the shell side and the tube side, respectively. The final heat carried by the circulating water is dissipated to environment by the WCT, in which the water is sprayed into droplets in the tower filling zone and exchanges heat with the air due to the mass transfer induced evaporative effect [37]. The water is collected in the bottom pool of the tower, and re-pumped into the STHE. Because the water mass may lose during the evaporative process, fresh water may be added into the system to ensure constant flow rate in the STHE.

# 2.2.1. The STHE simulation

Fig. 2 shows the basic type E STHE, belonging to the Tubular Exchanger Manufactures Association (TEMA) family. The  $\mathrm{CO}_2$  flows in the tube bundles from left to right, while the water flows in the shell side from right to left, waving its roadmap by periodically arranged baffles. Various design parameters of the STHE are listed in Table 2. The



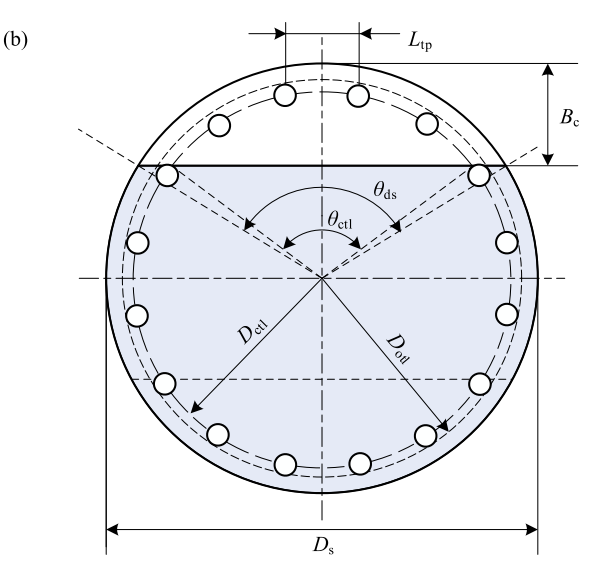


Fig. 2. Flow path and geometrical parameters of shell-tube-heat-exchanger.

**Table 2** Parameters of the shell-tube-heat-exchanger.

parameters	values
inner diameter of the shell, D <sub>s</sub>	1.5 m
outer diameter of the tube, $d_0$	25 mm
inner diameter of the tube $d_i$	22.2 mm
length of the tube, $L_{\rm t}$	10 m
thermal conductivity of the tube material, $k_{\rm t}$	50 W/mK
flow rate of cooling $CO_2$ , $m_{CO2}$	1615.1 kg/s
flow rate ratio of cooling $CO_2$ , $x_{c,s}$	71.5 %
outlet temperature of $CO_2$ , $T_s$	33 °C
outlet pressure of CO <sub>2</sub> , P <sub>s</sub>	7.6 MPa

**Table 3** Pressure loss coefficients for the shell-tube-heat-exchanger [55].

loss coefficient	calculation equation
heat transfer correction factor of baffle structure, $J_c$	$J_{\rm c} = 0.55 + 0.72F_{\rm c}$
correction factor for heat transfer of leakage between baffles, $J_1$	$\begin{split} J_{l} &= 0.44(1-r_{s}) + [1-0.44(1-r_{s})] exp(-2.2r_{lm}) \; r_{s} = \\ \frac{A_{o,sb}}{A_{o,sb} + A_{o,tb}}, \; r_{lm} &= \frac{A_{o,sb} + A_{o,tb}}{A_{o,cr}} \end{split}$
correction factor for pressure drop of leakage between baffles, R <sub>1</sub>	$R_1 = \exp[-1.33(1+r_s)]r_{\text{lm}}^x, x = -0.15(1+r_s+0.8)$
correction factor for heat transfer of bypass flow $J_b$ correction factor for	$J_b = \exp\{-C_{bh}F_{sbp}\left[1-(2r_{ss})^{\frac{1}{3}}\right]\}, r_{ss} = \frac{N_{ss}}{N_{tcc}}, \text{ laminar}$ flow $Res < 100, C_{bh} = 1.25, \text{ turbulent flow } C_{bh} = 1.35$
pressure drop of bypass flow, R <sub>b</sub>	$R_{\rm b}=\exp\left[-C_{\rm bp}F_{\rm sbp}(1-r_{\rm ss}^{-\frac{3}{3}})\right]$ , laminar flow Res<100, $C_{\rm bp}=1.25$ , turbulent flow $C_{\rm bp}=1.35$
correction factor for heat transfer of inlet and outlet baffles, $J_s$	The spacing between the inlet and outlet baffles in this article is kept consistent with the spacing between the other baffles., $J_s=1$
correction factor for pressure drop of inlet and outlet baffles, $R_s$	$R_{\rm s}=2$

calculations of the STHE involves the following processes (see Fig. S1 in the supplementary materials):

- Giving the thermal load of the cooler (Q<sub>c</sub>), the dimensions of the STHE, and the temperature and pressure values of the two sides of fluids.
- Assuming the dimensions of  $B_c$ ,  $L_{bc}$ ,  $L_{tp}$ ,  $N_{ss}$  and the outlet temperature of water  $(T_{wo})$ .
- Calculating the correction factors, geometric parameters of baffles and tubes.
- Evaluating the geometric parameters to see if the requirement is met.
   If not, keeping the iterative process until the requirement is satisfied.
- ullet Determining  $T_{wo}$ , and comparing the values of the current iterative step and the previous step. If the residual error does not meet the requirement, keeping the iterative process.
- Calculating the capital cost of the STHE.
- Finalizing the parameters of sCO<sub>2</sub> and cooling water, costs and heat transfer rate.

The flow and heat transfer model using the Bell–Delaware method is applied to design the STHE [55]. The correlation developed by Yoon et al. [56] is used to calculate the Nusselt number for  $sCO_2$  flowing in tubes:

$$Nu_{\rm s} = aRe_{\rm s}^b Pr_{\rm s}^c \left(\frac{\rho_{\rm s,pc}}{\rho_{\rm c}}\right)^n,$$
 (5)

where Re, Pr and  $\rho$  are Reynolds number, Prandtl number and density, respectively, the subscript s means sCO<sub>2</sub>, pc stands for the pseudocritical point. If  $T_{\rm s} > T_{\rm pc}$  exists, a = 0.14, b = 0.69, c = 0.66, n = 0; if  $T_{\rm s} \le T_{\rm pc}$  exists, a = 0.013, b = 1.0, c = -0.05, n = 1.6.

The Churchill formula [57] is used to calculate the friction factor f for  $sCO_2$  flowing in tubes:

$$f_{s} = 8 \left\{ \left( \frac{8}{Re_{s}} \right)^{12} + \left[ 2.457 \ln \left( \frac{1}{\left( \frac{7}{Re_{s}} \right)^{0.9} + \frac{0.27e}{d_{i}}} \right)^{16} + \left( \frac{37530}{Re_{s}} \right)^{16} \right]^{-1.5} \right\}^{-\frac{1}{12}}$$

$$(6)$$

For water flowing in the shell side, the heat transfer coefficient  $h_{\rm w}$  is cited from Ref. [55].

$$h_{\rm w} = h_{\rm id} J_{\rm c} J_{\rm l} J_{\rm b} J_{\rm s} J_{\rm r},\tag{7}$$

where  $h_{\rm id}$  is the heat transfer coefficient for pure crossflow of an ideal tube bank (see Eq. (8)). The four correction factors of J can be seen in Table 3. The  $h_{\rm id}$  is

$$h_{\rm id} = \frac{j_{\rm id} m_{\rm w} c_{\rm p,w} P r_{\rm w}^{-\frac{2}{3}}}{A_{\rm w}},\tag{8}$$

where  $j_{\rm id}$  is the ideal Colburn j factor for the shell side (see Eq. (9)).  $M_{\rm w}$  is the mass flow rate of water,  $A_{\rm w}$  is the cross-sectional area between two baffles,  $c_{\rm p}$  is the specific heat capacity, the subscript w means water.

$$j_{\rm id} = 0.236 Re_{\rm w}^{-0.346} \tag{9}$$

The friction factor *f* for water flowing in the shell side is as follows:

$$f_{\rm w} = 0.56Re_{\rm w}^{-0.14} \tag{10}$$

The pressure drop of water on the shell side is as follows:

$$\Delta P_{\rm w} = \Delta P_{\rm cr} + \Delta P_{\rm window} + \Delta P_{\rm e} \tag{11}$$

$$\Delta P_{\rm cr} = (N_{\rm b} - 1)\Delta P_{\rm b,id} R_{\rm b} \tag{12}$$

$$\Delta P_{\text{window}} = \frac{(2 + 0.6 N_{\text{tcw}}) G_{\text{w}}^2}{2\rho_{\text{w}}} N_{\text{b}} R_{\text{l}}$$
(13)

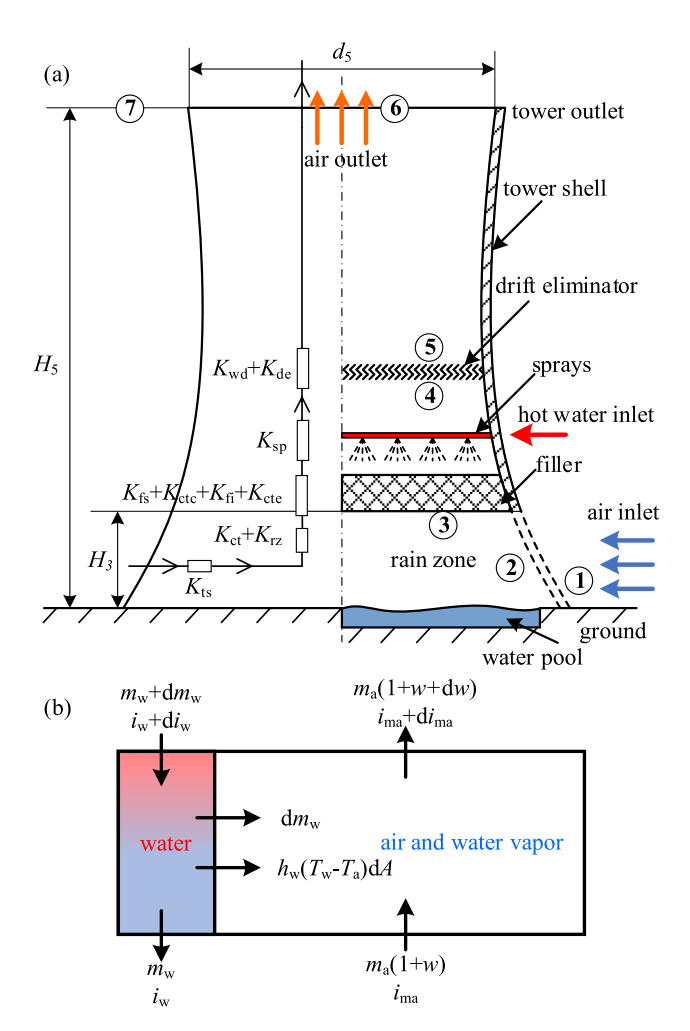
$$\Delta P_{\rm e} = 2\Delta P_{\rm b,id} R_{\rm b} R_{\rm s} \left( 1 + \frac{N_{\rm tcw}}{N_{\rm tcc}} \right) \tag{14}$$

$$\Delta P_{\text{b,id}} = \frac{2f_{\text{w}}N_{\text{tcc}}G_{\text{w}}^2}{\rho_{\text{w}}} \tag{15}$$

Where  $\Delta P_{\rm cr}$ ,  $\Delta P_{\rm window}$  and  $\Delta P_{\rm e}$  are the integrated pressure drops for all the interior crossflow sections, all window sections and that for the entrance and exit sections,  $\Delta P_{\rm b,id}$  is the ideal tube bank pressure drop, as specified in Ref. [55].  $N_{\rm b}$  is the number of baffles,  $N_{\rm tcw}$  is the effective number of tube rows crossed in the baffle window (see Eq. (16)),  $N_{\rm tcc}$  is the number of effective tube rows crossed in one crossflow section (see Eq. (17)), G is the mass flux of water. R is the non-ideal pressure drop coefficient (see Table 3). The  $D_{\rm s}$ ,  $D_{\rm ctl}$ ,  $B_{\rm c}$  and  $L_{\rm tp}$  are shown in Fig. 2.

$$N_{\text{tcw}} = \frac{0.8}{L_{\text{tp}}} \left( \frac{D_{\text{s}} B_{\text{c}}}{100} - \frac{D_{\text{s}} - D_{\text{ctl}}}{2} \right)$$
 (16)

1 1



 $\begin{tabular}{ll} Fig. & {\bf 3.} & {\bf Calculation} & {\bf models} & {\bf of} & {\bf the} & {\bf water-cooling-tower} & {\bf (a)} & {\bf and} & {\bf its} & {\bf filling} \\ {\bf zone} & ({\bf b}). & & & \\ \end{tabular}$ 

$$N_{\rm tcc} = -\frac{D_{\rm s}}{L_{\rm tp}} \left( 1 - \frac{2B_{\rm c}}{100} \right) \tag{17}$$

# 2.2.2. Simulation of the WCT

The WCT is divided into a spray zone, a filling zone, a rain zone, and a water reservoir (see Fig. 3). The circulating cooling water is sprayed into a mist through nozzles, exchanges heat with the air in the filling zone to decrease its temperature. The cooling capability of the WCT is limited by the wet bulb temperature of the environment air. The calculation process of the WCT is summarized here (see Fig. S2 in the supplementary materials):

- Specifying the parameters of the circulating water and the environmental air.
- ullet Assuming the parameters such as the tower height  $H_6$ , the air outlet temperature  $T_{a5}$ , the air flow rate  $m_a$ , and the air outlet pressure  $P_{a5}$ , etc.
- ullet Calculating the geometrical parameters of the cooling tower, the specific enthalpy of humid air  $i_{ma}$  at each marked position, and the flow resistance coefficients K.
- ullet Checking if the resistance equation is satisfied. If not, adjusting  $m_a$  until convergence.
- ullet Calculating the heat transfer rate and checking if the energy conservation equation and Merkel equation are satisfied. If not, adjusting  $T_{a5}$  and  $H_6$  until the requirements are met.
- Evaluating the cost of the WCT.

Pressure loss coefficients for the water-cooling-tower [37].

loss coefficient above the filler of spray zone, $K_{\rm spfi} \approx L_{\rm sp} \left[ \frac{1 - A_{\rm g}}{A_{\rm g}} \right] \left( \frac{m_{\rm mal}}{R_{\rm mal}} \right) \left( \frac{m_{\rm mal}}{R_{\rm mal}} \right)^2$ loss coefficient of water distribution system, $K_{\rm wdf} = 0.5 \left( \frac{M_{\rm mal}}{R_{\rm mal}} \right) \left( \frac{m_{\rm mal}}{R_{\rm mal}} \right)^2$	n loss of	$K_{gf} = \frac{G_{De}L_{g}d_{g}R_{g}^{2}}{(\pi d_{g}H_{g})^{2}} \times \frac{m_{mast}}{\rho_{mast}} \times \frac{m_{mast}}{\rho_{mast}}^{2}$ $K_{fif} = a_{il}R_{g}^{2} \left(\frac{n_{g}L_{g}d_{g}R_{g}R_{g}^{2}}{\rho_{mast}} \times \frac{m_{mast}}{\rho_{mast}}\right)^{2}$ $K_{fif} = a_{il}R_{g}^{2} \left(\frac{n_{g}L_{g}d_{g}R_{g}R_{g}^{2}}{\rho_{mast}} \times \frac{m_{mast}}{\rho_{mast}}\right)^{2}$ $K_{fif} = a_{il}R_{g}^{2} \left(\frac{n_{g}R_{g}^{2}}{\rho_{mast}} \times \frac{m_{mast}}{\rho_{mast}}\right)^{2} \times \frac{m_{mast}}{\rho_{mast}}$ $K_{fif} = a_{il}R_{g}^{2} \left(\frac{n_{g}R_{g}^{2}}{\rho_{mast}} \times \frac{n_{g}R_{g}^{2}}{\rho_{mast}} \times \frac{n_{g}R_{g}^{2}}{\rho_{mast}}\right)^{2} \times \frac{n_{g}R_{g}^{2}}{\rho_{mast}^{2}}$ $K_{fif} = \frac{G_{De}L_{g}d_{g}R_{g}^{2}}{\rho_{mast}^{2}} \left(\frac{n_{g}R_{g}^{2}}{\rho_{mast}^{2}} \times \frac{n_{g}R_{g}^{2}}{\rho_{mast}^{2}}\right)^{2} \times \frac{n_{g}R_{g}^{2}}{\rho_{mast}^{2}} \times \frac{n_{g}R_{g}^{2}}{\rho_{mast}^{2}} \left(\frac{n_{g}R_{g}^{2}}{\rho_{mast}^{2}} \times \frac{n_{g}R_{g}^{2}}{\rho_{mast}^{2}}\right)^{2} \times \frac{n_{g}R_{g}^{2}}{\rho_{mast}^{2}} \times \frac{n_{g}R_{g}^{2}}{\rho_{mast}^{2}} \left(\frac{n_{g}R_{g}^{2}}{\rho_{mast}^{2}} \times \frac{n_{g}R_{g}^{2}}{\rho_{mast}^{2}}\right)^{2} \times \frac{n_{g}R_{g}^{2}}{\rho_{mast}^{2}} \times \frac{n_{g}R_{g}^{2}}{\rho_{mast}^{2}} \left(\frac{n_{g}R_{g}^{2}}{\rho_{mast}^{2}} \times \frac{n_{g}R_{g}^{2}}{\rho_{mast}^{2}}\right) \left(\frac{n_{g}R_{g}^{2}}{\rho_{mast}^{2}}\right)^{2} \times \frac{n_{g}R_{g}^{2}}{\rho_{mast}^{2}} \left(\frac{n_{g}R_{g}^{2}}{\rho_{mast}^{2}} \times \frac{n_{g}R_{g}^{2}}{\rho_{mast}^{2}}\right) \left(\frac{n_{g}R_{g}^{2}}{\rho_{mast}^{2}}\right)^{2} \left(\frac$
loss coefficient of drift eliminator, $K_{\mathrm{defi}} = K_{\mathrm{defi}} = a_{\mathrm{de}} R_{\mathrm{de}}^{\lambda_{\mathrm{de}}} \left( \frac{\rho_{\mathrm{mat5}}}{\rho_{\mathrm{ma5}}} \right) \left( \frac{m_{\mathrm{ma5}}}{m_{\mathrm{ma15}}} \right)^2$		$K_{ ext{defi}} = a_{ ext{de}} R_{ ext{de}}^{V_{ ext{de}}} \left( rac{ ho_{ ext{ma15}}}{ ho_{ ext{ma15}}}  ight) \left( rac{m_{ ext{ma15}}}{m_{ ext{ma15}}}  ight)^2$

ullet Finalizing the outlet temperature  $T_{\rm w2}$  of the cooling water, heat transfer rate, and the WCT cost.

The following assumptions are made: (1) uniform water flow in the horizontal direction; (2) varied water flow in the vertical direction along the flow direction; (3) no blockage in the filling zone; (4) uniform air distribution in the horizontal direction. Flow resistance exists as the air flows upward, which is predicted as [37]:

air equals to that released by the cooling water:

$$m_{\rm a}(i_{\rm ma5}-i_{\rm ma1})=m_{\rm w}c_{\rm p,wm}(T_{\rm wi}-T_{\rm wo}),$$
 (21)

where  $i_{ma5}$  is the outlet enthalpy of the air,  $i_{ma1}$  is the inlet enthalpy of the air. Assuming that the air leaving the filling zone reaches the saturation state with the water-vapor, the Merkel equation is applied over the entire area between the inlet of the rain zone and the outlet of the spray zone [37]:

$$\begin{split} P_{a} \Big\{ \big[ 1 - 0.00975 \big( H_{3} + L_{fi}/2 \big) \big/ T_{a1} \big]^{3.5(1+w_{1})[1-w_{1}/(w_{1}+0.62198)]} \times \big\{ 1 + \xi_{Ta5} \big( H_{6} - H_{3} - L_{fi}/2 \big) \big/ T_{a5} \big\}^{-0.021233(1+w_{1}) \big/ \big[ \xi_{Ta_{5}}(w_{5}+0.622) \big]} \\ - (1 - 0.00975 H_{6}/T_{a1})^{3.5(1+w_{1})[1-w_{1}/(w_{1}+0.62198)]} \\ - \big( 0.02Fr_{D}^{-1.5} - 0.14 \big/ Fr_{D} \big) \big( m_{ma5}/A_{6} \big)^{2} \Big/ \rho_{ma6} \Big\} \\ = \big( K_{ts} + K_{il} + K_{ct} + K_{rz} + K_{fs} + K_{ctc} + K_{fi} + K_{cte} + K_{sp} + K_{wd} + K_{de} \big)_{fi} \\ \big( m_{ma15}/A_{fi} \big)^{2} \Big/ (2\rho_{a15}) \times \big[ 1 + \xi_{Ta5} \big( H_{6} - H_{3} - L_{fi}/2 \big) \big/ T_{a5} \big]^{-0.021233(1+w_{1}) \big/ \big[ \xi_{Ta_{5}}(w_{5}+0.622) \big]} + \alpha_{e6} \big( m_{ma5}/A_{6} \big)^{2} \Big/ (2\rho_{ma6} \big) \end{split}$$

where H is the height of different positions of the WCT,  $L_{\rm fi}$  is the height of the filling zone, which is 2.0 m in this paper,  $T_{\rm a1}$  is the ambient air temperature (see Fig. 3), w is the humidity ratio,  $\rho$  is the density, m is the mass flow rate,  $A_{\rm fi}$  is the frontal area of the filling zone. The subscripts a and ma indicate the dry air and the moist air, respectively. The subscripts 1, 3, 5, 6 represent the parameters at the position marked 1, 3, 5 and 6 in Fig. 3, respectively. K is the dimensionless resistance coefficient (see Table 4). The  $\xi_{\rm Ta5}$  is the lapse rate for this condensation process [37], in Eq. (19).

$$\xi_{\text{Ta5}} = \frac{-(1+w_5)g\left\{1 + 0.42216 \times 10^{-11}w_5^2 P_{\text{a5}} \exp\left(\frac{5406.1915}{T_{\text{a5}}}\right) \frac{i_c}{(w_5 + 0.622)RT_{\text{a5}}}\right\}}{c_{\text{p,ma}} + 3.6693 \times 10^{-8}w_5^2 P_{\text{a5}} \exp\left(\frac{5406.1915}{T_{\text{a5}}}\right) \frac{i_c}{T_{\text{a5}}^2}},$$
(19)

$$Me = \frac{h_{\rm d}aL}{G_{\rm w}} = \int_{T}^{T_{\rm wi}} \frac{c_{\rm p,w}dT_{\rm w}}{(i_{\rm masw} - i_{\rm ma})}$$
 (22)

$$\frac{h_{\rm d}aL}{G_{\rm w}} = \frac{h_{\rm drz}a_{\rm rz}L_{\rm rz}}{G_{\rm w}} + \frac{h_{\rm dfi}a_{\rm fi}L_{\rm fi}}{G_{\rm w}} + \frac{h_{\rm dsp}a_{\rm sp}L_{\rm sp}}{G_{\rm w}}, \tag{23}$$

Where the non-dimensional term  $\frac{h_a a L}{G_w}$  is called the Merkel number (Me),  $h_d$  is the mass transfer coefficient, a is the wetted area divided by the volume of different zones, L is height of different zones, the subscript masw means the saturated moist air. The Merkle number in the rain zone, filling zone and spray zone is expressed as follows:

$$\begin{split} \frac{h_{\rm drz} a_{\rm rz} L_{\rm rz}}{G_{\rm w}} &= 12 \bigg( \frac{\lambda_1}{\nu_{\rm ma3} d_{\rm d}} \bigg) \bigg( \frac{H_3}{d_{\rm d}} \bigg) \bigg( \frac{P_{\rm a1}}{R_{\rm v} T_{\rm a1} \rho_{\rm wo}} \bigg) Sc_1^{0.33} \bigg[ \ln \bigg( \frac{w_{\rm s1} + 0.622}{w_1 + 0.622} \bigg) \frac{1}{(w_{\rm s1} - w_1)} \bigg] \times \big\{ 0.90757 a_{\rm p} \rho_{\it ma1} - 30341.04 a_{\rm p} \mu_{\it ma1} - 0.37564 \\ &+ 4.04016 \big\{ [0.55 + 41.7215 \times (a_{\rm L} d_{\rm d})^{0.80043} \big] \big[ 0.713 + 3.741 (a_{\rm L} H_3)^{-1.23456} \big] \big[ 3.11 \exp(0.15 a_{\rm v} \nu_{\rm ma3}) - 3.13 \big] \\ &\times \exp \big\{ [5.3759 \exp(-0.2092 a_{\rm L} H_3)] \ln[0.3719 \exp(0.0019055 a_{\rm L} d_3) + 0.55] \big\} \big\} \big\} \end{split}$$

Where 
$$i_e = i_{fgwo} - (c_{p,w} - c_{p,v})(T_{a5} - 273.15)$$
. The  $Fr_D$  is [37]
$$Fr_D = (m_{ma5}/A_6)^2 / [\rho_{ma6}(\rho_{ma7} - \rho_{ma6})gd_6]$$
(20)

The filling zone of the WCT is an important region for heat transfer between the air and the water, with the calculation model shown in Fig. 3b. Based on energy conservation, the energy absorbed by the moist

**Table 5**Design parameters of water-cooling-tower.

cooling tower parameters	values
ambient temperature, $T_{\rm a}$	20.0 °C
local air pressure, Pa	101.305 kPa
relative humidity, RH	70 %
net power, $W_{\text{net}}$	300 MW
cooling water flow rate in the cooling tower, $m_{\rm w}$	3860 kg/s
ratio of tower height to tower inlet diameter	1.4
ratio of tower inlet and outlet diameter	0.7
ratio of tower inlet diameter to inlet height	9

$$\frac{h_{\rm dfi}a_{\rm fi}L_{\rm fi}}{G_{\rm w}} = 0.25575L_{\rm fi}G_{\rm w}^{-0.094}G_{\rm a}^{0.6023} \tag{25}$$

$$\frac{h_{\rm dsp}a_{\rm sp}L_{\rm sp}}{G_{\rm w}} = 0.2L_{\rm sp} \left(\frac{G_{\rm a}}{G_{\rm w}}\right)^{0.5},\tag{26}$$

where the  $d_{\rm d}$  is the mean diameter of the water droplet in rain zone,  $d_{\rm d}=0.0035$  m,  $\lambda$  is the diffusion coefficient at inlet,  $\nu$  is the velocity,  $\mu$  is the dynamic viscosity. The Schmidt number  $Sc_1$  is

$$Sc_1 = \mu_{ma1} / (\rho_{ma1}\lambda_1), \tag{27}$$

where the  $\mu$  is the dynamic viscosity, several coefficients of a in Eq. (24) are shown in Eqs. (28)–(31).

$$a_{\mu} = 3.031 \times 10^{-6} \left( \rho_{wo}^4 g^9 / s_{wo} \right)^{0.25}$$
 (28)

$$a_{p} = 998.0/\rho_{wo}$$
 (29)

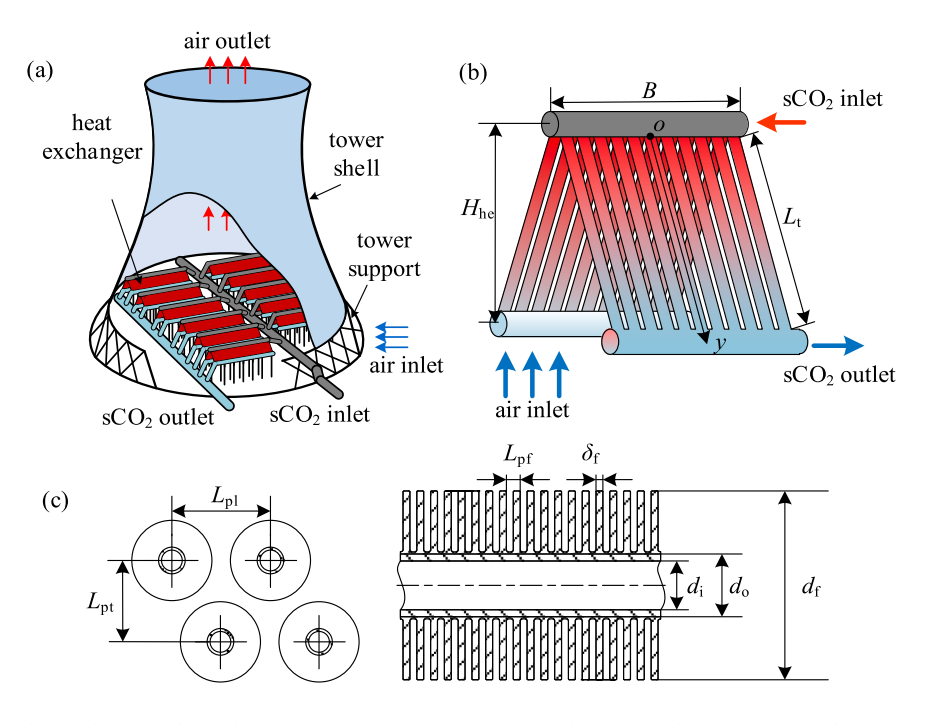


Fig. 4. Physical models of the air-cooler and the A-type heat exchanger, (a) air-cooling-tower, (b) A-type heat exchanger, and (c) finned-tube.

$$a_{\rm v} = 73.298 \left(g^5 \sigma_{\rm wo}^3 / \rho_{\rm wo}^3\right)^{0.25} \tag{30}$$

$$a_{\rm L} = 6.122 (g\sigma_{\rm wo}/\rho_{\rm wo})^{0.25},$$
 (31)

where  $\sigma$  is the surface tension of water, the subscript wo means the outlet water. The design parameters of water-cooling tower are shown in Table 5.

# 2.2.3. The economic model of the water cooler

The cost of the water cooler is divided into two parts: the cost of the STHE and the cost of the WCT. The later consists of the cost of the tower body and the cost of the filler.

$$C_{\text{cooler}} = C_{\text{tower}} + C_{\text{shell-tube}} + C_{\text{fi}}, \tag{32}$$

where C represents the cost, the subscripts fi represents the filler.

The  $C_{\rm shell-tube}$  is calculated based on Ref. [58]. The unit is US dollar for such calculation but is converted into Chinese Yuan here, according to the exchange rate of 7.23. The carbon steel is selected as the construction material.

$$C_{\text{shell-tube}} = 7000 + 360 A_{\text{shell-tube}}^{0.8},$$
 (33)

where  $A_{\text{shell-tube}}$  is the heat transfer area of the shell-tube-heat-exchanger. The tower cost  $C_{\text{tower}}$  is

$$C_{\text{tower}} = V_{\text{shell}} c_{\text{shell}} \tag{34}$$

$$C_{\rm fi} = V_{\rm fi}c_{\rm fi},\tag{35}$$

where  $c_{\rm shell}$  is the investment per unit volume of the tower shell, which is 200 \$/m³,  $c_{\rm fi}$  is the investment per unit volume of the filler [59], which is 25 \$/m³,  $V_{\rm shell}$  and  $V_{\rm fi}$  are the volumes of the tower shell and the filler, respectively.

# 2.3. Air-cooler

The air-cooler (AC) uses nature air to dissipate heat of the  $CO_2$  fluid (see Fig. 4a). The ACT is divided into an air inlet region, a heat transfer region and an air outlet region. The circulation of air is caused by the

buoyancy effect due to the air temperature difference between the outlet region and the inlet region. The finned tube heat exchanger is crucial to dominate the AC performance, consisting of a set of units (see Fig. 4b–c). These units are horizontally and parallelly positioned in the heat transfer region. Each heat exchanger unit displays the triangular configuration. The  $\rm CO_2$  fluid enters the parallel tubes via the upper plenum, flows in the tube bundle and dissipates heat to the air there, and then collects in the bottom plenum. The finned tubes enhance the convective heat transfer in the air side.

# 2.3.1. Calculation model of the air-cooler

The simulation of the air-cooler includes the geometrical parameters of the AC, the heat transfer rate of the heat exchangers, and the cost of the AC (see Fig. S3 in the supplementary materials). The calculation process is summarized are as follows.

- Assuming the height of the air-cooling-tower (ACT) and the outlet air temperature of the heat exchangers.
- Determining the air flow rate based on the flow resistance calculation of the air.
- Updating the outlet air temperature based on the heat transfer between the sCO<sub>2</sub> and the air.
- Iterating the outlet air temperature to obtain the outlet parameters of sCO<sub>2</sub> until convergence.
- Comparing the outlet parameters of sCO<sub>2</sub> with the cycle specified values, changing the height of the tower until the outlet parameters of sCO<sub>2</sub> are equal to the design values.
- Calculating the cost of the ACT.

It is noted that the air flow is caused by the buoyancy effect, creating the driving force to overcome the flow resistance of the air flowing through the ACT (see Fig. 5a). The flow resistance is calculated based on the Konger's theory [37]:

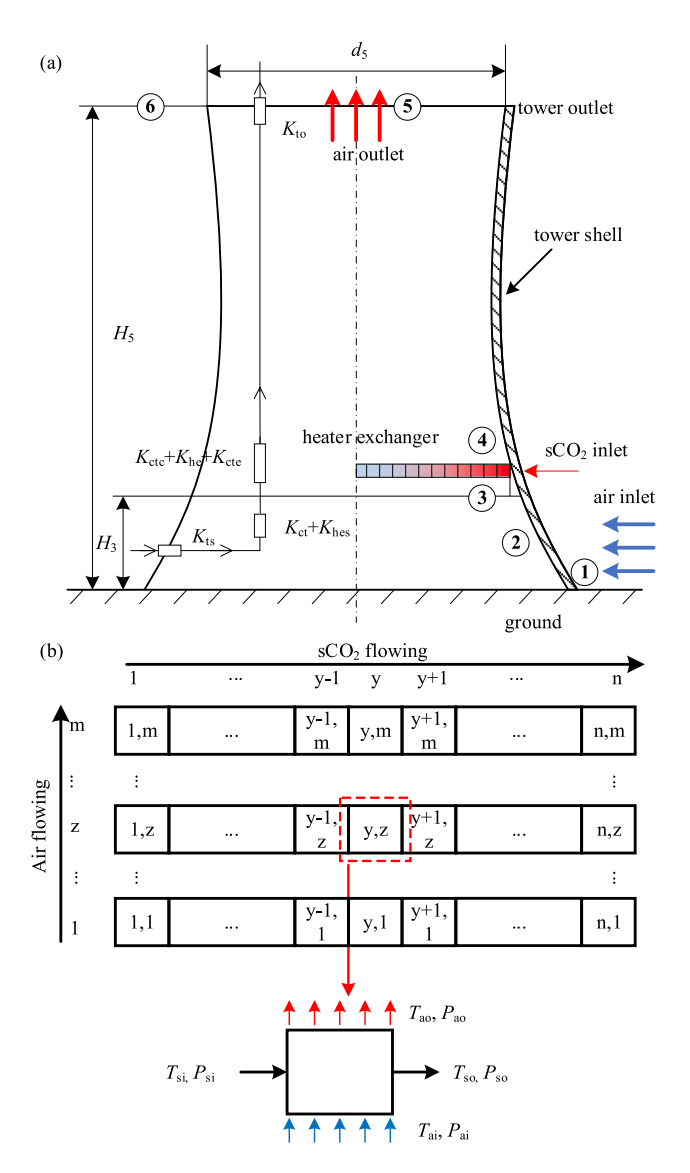


**Fig. 5.** Calculation model of the air-cooling-tower and the A-type heat exchanger.

**Table 6**Pressure loss coefficients for the air-cooling-tower [37].

	-
loss coefficient	calculation equation
loss coefficient of tower support, $K_{ts}$	$K_{\mathrm{ts}} = rac{C_{\mathrm{Dts}}L_{\mathrm{ts}}d_{\mathrm{ts}}n_{\mathrm{ts}}A_{\mathrm{fr}}^2}{\left(\pi d_{3}H_{3} ight)^{3}}\left(rac{ ho_{\mathrm{a34}}}{ ho_{\mathrm{a1}}} ight)$
contraction loss coefficient, $K_{\rm ctc}$	$K_{\mathrm{ctc}} = \left(1 - \frac{2}{\sigma_{\mathrm{c}}} - \frac{1}{\sigma_{\mathrm{c}}^2}\right) \left(\frac{\rho_{\mathrm{a34}}}{\rho_{\mathrm{a3}}}\right) \left(\frac{A_{\mathrm{fr}}}{A_{\mathrm{e3}}}\right)^2$
expansion loss coefficient, $K_{\text{cte}}$	$K_{\mathrm{cte}} = \left(1 - rac{A_{\mathrm{fr}}}{A_{3}} ight)^{2} \left(rac{ ho_{\mathrm{a34}}}{ ho_{\mathrm{a4}}} ight) \left(rac{A_{\mathrm{fr}}}{A_{\mathrm{e3}}} ight)^{2}$
loss coefficient of cooling tower inlet, $K_{ct}$	$K_{\rm ct} = K_{\rm cthe} \left(\frac{\rho_{\rm a34}}{\rho_{\rm a1}}\right) \left(\frac{A_{\rm fr}}{A_{\rm 3}}\right)^2,$
	$K_{\text{cthe}} = 0.072 \left(\frac{d_3}{H_3}\right)^2 - 0.34 \left(\frac{d_3}{H_3}\right) - 1.7$
loss coefficient of cooling tower	$K_{\text{to}} = -0.28 F r_D^{-1} + 0.04 F r_D^{-1.5},$
outlet, $K_{to}$	$Fr_D = \frac{1}{ ho_{a5}( ho_{a6} -  ho_{a5})gd_5} \left(\frac{m_a}{A_5}\right)^2$
loss coefficient of heat exchanger, $K_{ m he}$	$K_{\text{he}} = \frac{13893.94795}{Ry^{0.332458}} + \frac{2}{\sigma^2} \frac{\rho_{\text{a3}} - \rho_{\text{a4}}}{\rho_{\text{a3}} + \rho_{\text{a4}}}, Ry =$
	$rac{m_{ m a}}{\mu_{ m a34}A_{ m fr}}$

**Table 7**Geometrical parameters of finned-tube-heat-exchanger.

tube parameters	value	fin parameters	value
- tube parameters		im parameters	
tube material	ASTM A214	fin material	ASTM 6063
	low carbon		aluminum
	steel		
thermal conductivity of	50 W/mK	number of tube	1
tube, $k_{\rm t}$		passes, $n_{\rm wp}$	
outer diameter of the	19 mm	thermal	204 W/(m K)
tube, $d_{\rm o}$		conductivity of fin,	
		$k_{ m f}$	
inner diameter of the	14 mm	fin diameter, $d_{ m f}$	57 mm
tube, $d_{\rm i}$			
relative roughness of	$5.24 \times 10^{-4}$	finned cross-	conical
the tube surface, $\varepsilon/d_{ m i}$		sectional shape	
length of the tubes, $L_{\rm t}$	6 m	average fin	0.5 mm
		thickness, $\delta_{\mathrm{f}}$	
number of tubes per	46	fin spacing, $L_{\rm pf}$	2.8 mm
row, $n_{\rm tr}$			
transverse tube spacing,	58		
$L_{ m pt}$			
longitudinal tube	52		
spacing, $L_{ m pl}$			
width of each heat	$H_3/1.15$		
exchanger, $B_{he}$			
height of each heat	0.5 m		
exchanger, $H_{he}$			

$$\begin{split} &P_{a}\Big\{[1-0.00975(H_{3}+H_{4})/(2T_{a1})]^{3.5}\\ &\times[1-0.00975(H_{5}-H_{3}/2-H_{4}/2)/T_{a4}]^{3.5}-(1-0.00975H_{5}/T_{a1})^{3.5}\Big\}\\ &=(K_{ts}+K_{ctc}+K_{hes}+K_{ct}+K_{he}+K_{cte})_{he}\big(m_{a}/A_{fr}\big)^{2}\Big/(2\rho_{a34}\big)\\ &\times[1-0.00975(H_{5}-H_{3}/2-H_{4}/2)/T_{a4}]^{3.5}+(1+K_{to})(m_{a}/A_{5})^{2}\Big/(2\rho_{a5}) \end{split} \label{eq:partial_equation}$$

where H is the height of different positions of the ACT,  $T_{a1}$  is the ambient air temperature (see Fig. 5),  $\rho$  is the density, m is the mass flow rate,  $A_{\rm fr}$  is the frontal area of the finned tube heat exchanger. The subscripts a and ma indicate the dry air and the moist air, respectively. The subscripts 1, 3, 4 and 5 represent the parameters at the position marked 1, 3, 4 and 5 in Fig. 5a. Various pressure loss coefficients K exist in Eq. (36), which can be seen in Table 6.

## 2.3.2. The heat transfer model of the ACT

The heat exchangers are arranged in multiple rows. Compared with the inline arrangement, the staggered arrangement has better heat transfer performance and adopts a single tube pass. Due to the poor heat transfer of the air, the welding circular fins on the tube surface enhances heat transfer (see Fig. 4c). The geometrical parameters of the finned tube heat exchanger are shown in Table 7.

The calculation of the finned tube heat exchanger adopts the Konger's model [37]. Each finned tube is divided into several nodes along the length direction. For a single node, the heat transfer rate on the air side and the  $sCO_2$  side are  $Q_a$  and  $Q_s$ , respectively (see Fig. 5b). Eqs.(35) and (36) calculate  $Q_a$  and  $Q_s$  based on the enthalpy change across the inlet and outlet of the node, respectively. The two values are equal to the heat transfer calculation  $Q_{he}$ .

$$Q_{a} = m_{a}c_{p,a}(T_{a,y+1} - T_{a,y})$$
(37)

$$Q_{s} = m_{s}c_{p,s}(T_{s,y+1} - T_{s,y})$$
(38)

$$Q_{\text{he}} = UAF_{\text{T}} \frac{\left(T_{\text{s,y}} - T_{\text{a,y+1}}\right) - \left(T_{\text{s,y+1}} - T_{\text{a,y}}\right)}{\ln\left(\frac{T_{\text{s,y}} - T_{\text{a,y+1}}}{T_{\text{s,y+1}} - T_{\text{a,y}}}\right)},$$
(39)

where UA is the overall heat transfer coefficient,  $F_T$  is the heat transfer area, the last term in Eq. (39) is the logarithmic mean temperature

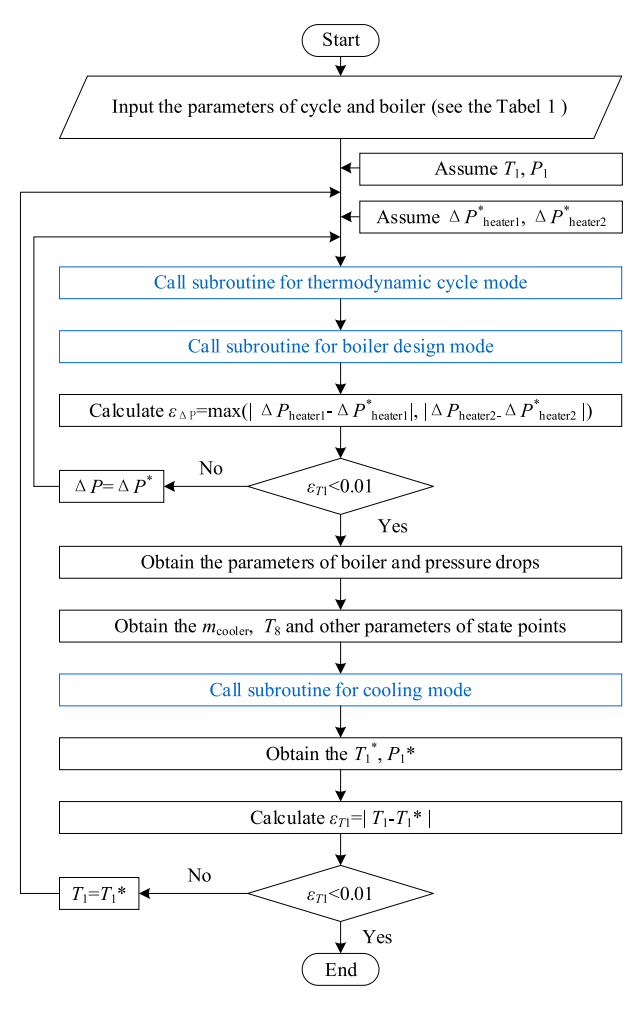


Fig. 6. Calculation flow-chart of the sCO2 coal-fired power generation system.

**Table 8**Model validation for the water-cooling tower.

parameters	present study	Ref. [37]
$m_{ m w}$	12500 kg/s	12500 kg/s
$m_a$	16522.44 kg/s	16522.46 kg/s
$T_{wi}$	40 °C	40 °C
$T_{ m wo}$	21.39 °C	21.39 °C
$Q_{\mathrm{w}}$	972.06 MW	972.06 MW
$Q_{\rm a}$	971.97 MW	972.06 MW

difference (LMTD), m is the mass flow rate,  $c_p$  is the specific heat, and T is the temperature, the subscripts a and s stand for air and sCO<sub>2</sub>, respectively, y and y+1 represent the parameters at the node y and the right node y+1, respectively. The UA is

$$UA = \left[\frac{1}{h_{s}A_{s}} + \frac{1}{2\pi k_{t}n_{b}n_{t}\Delta L}\ln\frac{d_{o}}{d_{i}} + \frac{1}{2\pi k_{f}n_{b}n_{t}\Delta L}\ln\frac{d_{f}}{d_{o}} + \frac{1}{h_{a}A_{a}}\right]^{-1},$$
 (40)

where  $h_s$  and  $h_a$  are the convective heat transfer coefficients for sCO<sub>2</sub> and air, respectively, A represents the heat transfer area,  $k_t$  and  $k_f$  are the thermal conductivities of the tube and the fin, respectively,  $n_b$  is the number of heat transfer tube bundles,  $n_t$  is the number of tubes per bundle, and  $\Delta L$  is the length of the calculation node.

Briggs and Young [60] proposed the heat transfer correlation of air for fin-tube-heat-exchanger with staggered tube banks.

$$\frac{h_{\rm a}d_{\rm o}}{k_{\rm a}} = 0.134 Pr_{\rm a}Re_{\rm a} \left[\frac{2\left(L_{\rm pf}-t_{\rm f}\right)}{d_{\rm f}-d_{\rm o}}\right]^{0.2} \left(\frac{L_{\rm pf}-\delta_{\rm f}}{\delta_{\rm f}}\right)^{0.1134},\tag{41}$$

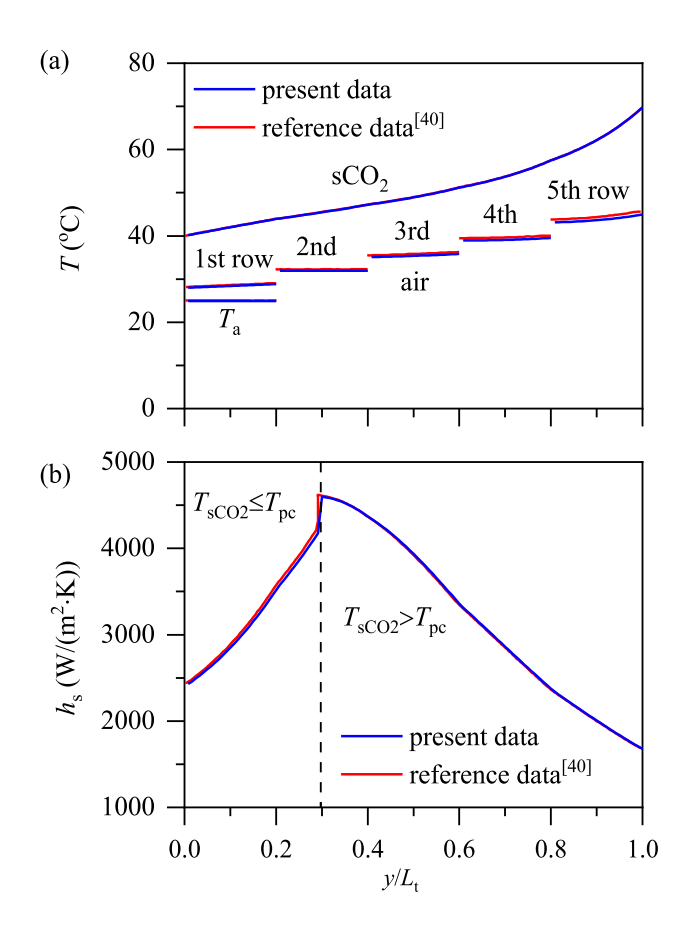


Fig. 7. Model validation for air-cooler.

Table 9
Parameters for the coolers.

water-cooled	values	air-cooled	value
Water-cooled tower		tower height, H <sub>5</sub>	130.0 m
height of tower, $H_6$	130.0 m	height of tower inlet, $H_3$	10.3 m
height of tower inlet, $H_3$	10.3 m	diameter of tower inlet, $d_3$	92.9 m
diameter of tower inlet, $d_3$	92.9 m	diameter of tower outlet, $d_5$	65 m
diameter of tower outlet, $d_6$	65 m	number of cooling tube bundle, $n_b$	260
height of filler	2.0 m	air flow rate, ma	17701.0
-			kg/s
air flow rate, $m_{\rm a}$	11400 kg/s	cooling capacity, $Q_{\rm cooler}$	298.7 MW
cooling capacity, $Q_{cooler}$	299.5	CO2 cooling flow rate	1652.1 kg/
	MW		s
Shell and tube heat exchanger		$CO_2$ cooling flow rate ratio, $x_{c.s}$	73.2 %
baffle clearance, $B_c$	0.37 m	$CO_2$ outlet temperature, $T_s$	34.2 °C
baffle spacing, $L_{ m bc}$	0.45 m	CO2 outlet pressure, Ps	7.6 MPa
tube pitch, $L_{\rm tp}$	0.032 m	net power, $W_{\text{net}}$	291.5 MW
inlet temperature of circulating water, $T_{wi}$	23.8 °C		
outlet temperature of circulating water, $T_{wo}$	43.2 °C		
number of shell and tube heat exchangers	10		

Where the Reynolds number  $Re_a = G_a d_o/\mu_a$ . Eq. (41) is valid under the conditions of  $1000 < {\rm Re_a} < 18000$ ,  $11.013~{\rm mm} < d_o < 40.89~{\rm mm}$ ,  $1.42~{\rm mm} < (d_{\rm f} \cdot d_o)/2 < 16.57~{\rm mm}$ ,  $0.33~{\rm mm} < \delta_{\rm f} < 2.02~{\rm mm}$ ,  $1.30~{\rm mm} < L_{\rm pf} < 1.00~{\rm mm}$ 

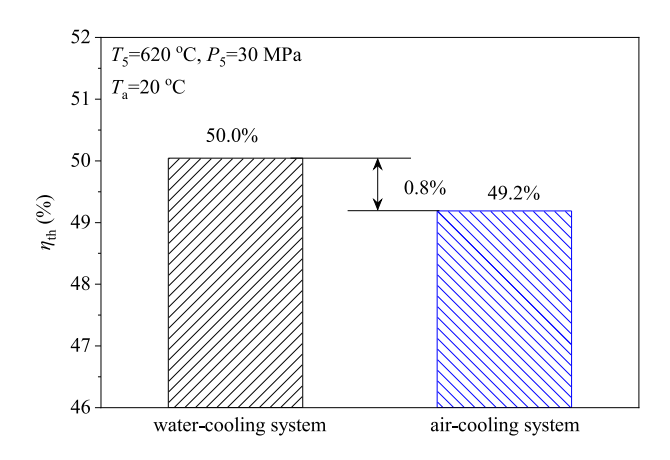


Fig. 8. Thermal efficiencies of the 300 MW  $sCO_2$  power generation systems using water-cooler and air-cooler.

# 4.06 mm, and 24.49 mm $< L_{pt} < 111$ mm.

Robinson and Briggs [61] proposed the friction factor correlation of air for the heat exchanger.

$$f_{\rm a} = \frac{D_{\rm a}}{2L_{\rm pl}} f_{\rm RB} \tag{42}$$

$$f_{\rm RB} = 9.465 Re_{\rm a} \left(\frac{L_{\rm pt}}{d_{\rm o}}\right)^{-0.927} \left(\frac{L_{\rm pt}}{L_{\rm pl}}\right)^{0.515},$$
 (43)

where  $L_{\rm pl}$  and  $L_{\rm pt}$  are longitudinal tube spacing and transverse tube spacing, respectively,  $D_{\rm a}$  is the equivalent diameter of air flow,  $d_{\rm o}$  is the out diameter of tubes. Eqs.(42) and (43) are valid under the conditions of 2000<Re<sub>a</sub> < 50000, 18.64 mm <  $d_{\rm o}$  < 40.89 mm, 39.68 mm <  $d_{\rm f}$  < 69.85 mm, 10.52 mm< ( $d_{\rm f}$ - $d_{\rm o}$ )/2 < 14.48 mm, 42.85 mm <  $L_{\rm pt}$  <114.3 mm, and 37.11 mm <  $L_{\rm pl}$  <98.99 mm. The heat transfer coefficient and friction factor for sCO<sub>2</sub> flowing in tubes are shown in Eqs. (5) and (6), which are not repeated here. Thermal physical properties of sCO<sub>2</sub> are cited from the commercial software REFPROP 9.0 [62].

# 2.3.3. The economic model of the air-cooler

The capital cost of an air-cooler ( $C_{\rm cooler}$ ) consists of the construction cost of the tower body ( $C_{\rm tower}$ ) and the cost of the finned-tube-heat-exchanger ( $C_{\rm he}$ ):

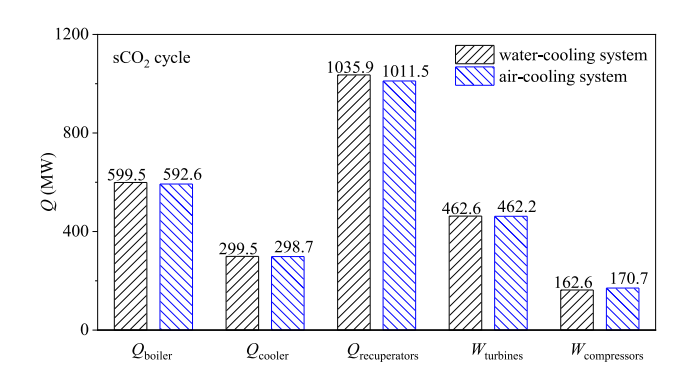


Fig. 10. Energy distribution in the water-cooling and air-cooling cycle.

$$C_{\text{cooler}} = C_{\text{tower}} + C_{\text{he}} \tag{44}$$

The right side of Eq. (44) is given by Eq. (34) and Eq. (45) [63], respectively.

$$C_{\text{he}} = c_{\text{he}} A_{\text{he}},\tag{45}$$

where  $c_{\text{he}}$  is the investment per unit area of the fined-tube-heat-exchanger, 11 \$/m<sup>2</sup> [63],  $A_{\text{he}}$  is the effective frontal area of the heat exchanger.

**Table 10** Physical properties of working fluids calculated by the NIST software [62].

	U		•	
	density (kg/m³)	specific heat capacity (kJ/kg K)	thermal conductivity (mW/(m K)	viscosity (μPa s)
cooling water (20 °C, 0.1 MPa)	998.21	4.1841	598.01	1001.6
cool air (20 °C, 0.1 MPa)	1.1888	1.0061	25.873	18.205
saturated water vapor (50°C, 5 kPa)	0.033578	1.8964	20.242	70.530
sCO <sub>2</sub> (33 °C, 7.6 MPa)	346.97	20.372	69.976	25.416
sCO <sub>2</sub> (100 °C, 7.6 MPa)	132.52	1.3036	27.967	20.273

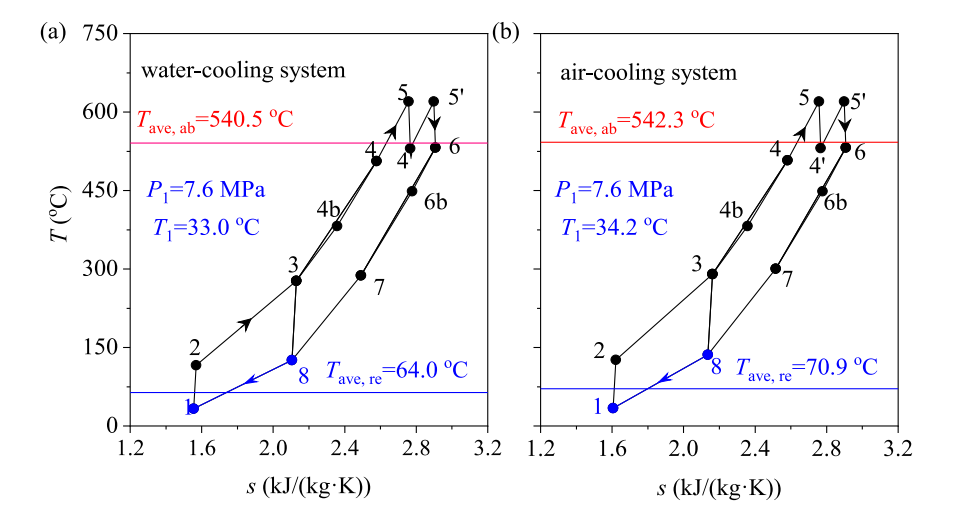


Fig. 9. T-s diagram of the sCO<sub>2</sub> cycle using water-cooler (a) and air-cooler (b).

#### 2.4. The coupling simulation of the cycle and the cooler

The correlations and equations presented in this paper were developed using air as the working medium. Notably, these equations have been successfully applied in studies on  $sCO_2$  coolers, as demonstrated in Refs. [38–42], highlighting their applicability beyond water-based systems.

In this paper, the  $sCO_2$  cycle is coupled with either the water-cooler or the air-cooler (see Fig. 6 for the coupling calculations of the cycle and the tower.) The detail cycle calculation and boiler design calculation can be seen in Ref.[30]. The model validation for water-cooler and air-cooler can be seen in Table 8 and Fig. 7.

#### 3. Results and discussion

In order to perform the comparative studies using the coolers, the height-to-diameter ratios of the two coolers are identical. The geometrical parameters of the water-cooler are calculated to obtain its parameters under the design conditions. Then, the parameters of the air-cooler are set to be identical to those of the water-cooling tower (see Table 9 for these parameters).

#### 3.1. Effect of air-cooler and water-cooler on the cycle performance

Thermal efficiency ( $\eta_{th}$ ) is a key index to evaluate the sCO<sub>2</sub> cycle performance, which is influenced by various factors. By setting identical design parameters such as the main vapor temperature  $T_5 = 620$  °C, the main vapor pressure  $P_5 = 30$  MPa and the air temperature of 20 °C, Fig. 8 plots the efficiencies of the power plants coupling with the air-cooler and the water-cooler. It is seen that the efficiencies reach 50.0 % and 49.2 % with the water-cooler and the air-cooler, respectively, indicating a 0.8 % efficiency penalty by using the air-cooler. In contrast, the efficiency penalty reaches 2.2 % for the water-steam Rankine cycle power plant by using the air-cooler instead of the water-cooler [45]. We conclude that the sCO<sub>2</sub> cycle has weaker efficiency plenty by using the air-cooler instead of the water-cooler than the water-steam Rankine cycle. This benefit comes from the fact that the temperature difference between the sCO<sub>2</sub> and the cooling fluids is larger than that between the water-vapor and the cooling fluids for the water-steam power plant, which will be discussed later.

For thermal engines, the average heat absorption temperature ( $T_{\rm ave,\ ab}$ ) reflects the coupling between the heat source and the cycle. Meanwhile, the average heat release temperature ( $T_{\rm ave,\ re}$ ) reflects the coupling between the cycle and the final heat sink [53,54]. The cycle efficiency is improved by elevating  $T_{\rm ave,\ ab}$  and/or lowering  $T_{\rm ave,\ re}$ . The

T-s diagrams for the cycles using the water-cooler and the air-cooler are shown in Fig. 9, where s is the entropy. It is seen that compared with the water-cooler, the air-cooler not only increases  $T_{\rm ave,\ ab}$  by  $\sim$ 2 K, but also increases  $T_{\rm ave,\ re}$  by  $\sim$ 7 K. The comprehensive effect introduces a 0.8 % cycle efficiency difference of the cycles between using the air-cooler and the water-cooler.

Due to the different cooling performance of the two cooling methods, it can be seen in Fig. 9, the  $T_1$  for water-cooling system and air-cooling system is 33 °C and 34.2 °C, respectively. Increasing the inlet temperature of the compressor will increase its power consumption. The output power of turbine for water-cooling system and air-cooling system is 462.6 MW and 462.2 MW, respectively (see Fig. 10). The compressor power consumption for water-cooling system and air-cooling system is 163 MW and 171 MW, respectively (see Fig. 10). Therefore, the net power of the water-cooling sCO<sub>2</sub> cycle is 300 MW, while the net power of the air-cooling sCO<sub>2</sub> cycle is 291.5 MW.

## 3.2. Heat transfer behavior of the air-cooler and the water-cooler

Here, a short review is given on the heat carrier fluid to be cooled by the cooler, which is  $sCO_2$  for the  $sCO_2$  cycle and water-vapor for the Rankine cycle. For the  $sCO_2$  cycle, heat transfer takes place due to sensible heat release in supercritical pressure, but due to latent heat dissipation in subcritical pressure for the Rankine cycle. This difference influences the heat transfer roadmaps in the coolers, creating different effect of the coolers on the power generation systems.

Now we turn to analyze the effect of cooling fluids on the  $sCO_2$  cycle. The physical properties of air and water are obviously different (see Table 10). At atmospheric pressure and the temperature of 20 °C, the density of water is three magnitudes larger than that of air. Meanwhile, the special heat and the thermal conductivity of water are four times and twenty-three times of air, respectively. These differences result in significant different heat transfer behavior between air and water.

Fig. 11 illustrates the T- $\Delta H$  diagram for the STHE and the air-cooler, where  $\Delta H$  is the enthalpy change along the heat transfer roadmaps. The pinch temperature is defined as the minimum temperature difference across the two sides of fluids along the whole heat transfer roadmap. It is seen that the pinch is located just before the sCO<sub>2</sub> leaves the STHE, which is 8.8 °C for water cooling (see Fig. 11a), but exactly located at the point 1 at the sCO<sub>2</sub> outlet, which is 14.2 °C for air cooling (see Fig. 11b). Having the temperatures of the four state points across the sCO<sub>2</sub> side and the cooling fluid side, the LMTD is determined to be 33.4 °C in the STHE, and 34.2 °C in the air cooler, indicating mini difference of the LMTD for the two coolers.

It is noted that the LMTD is only determined by the temperatures of

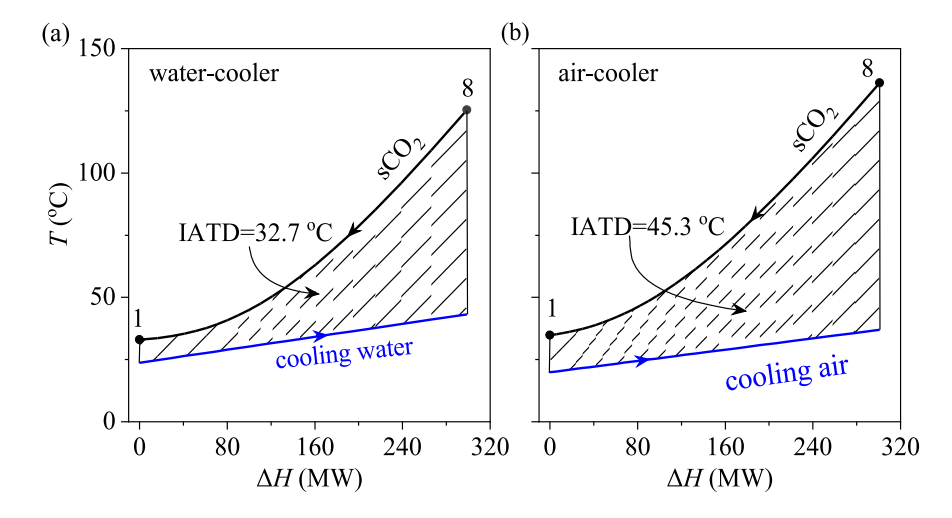


Fig. 11. T- $\Delta H$  diagram of the heat transfer roadmaps between the heat carrier fluid and the cooling fluid: (a) for the water-cooler, (b) for the air-cooler.

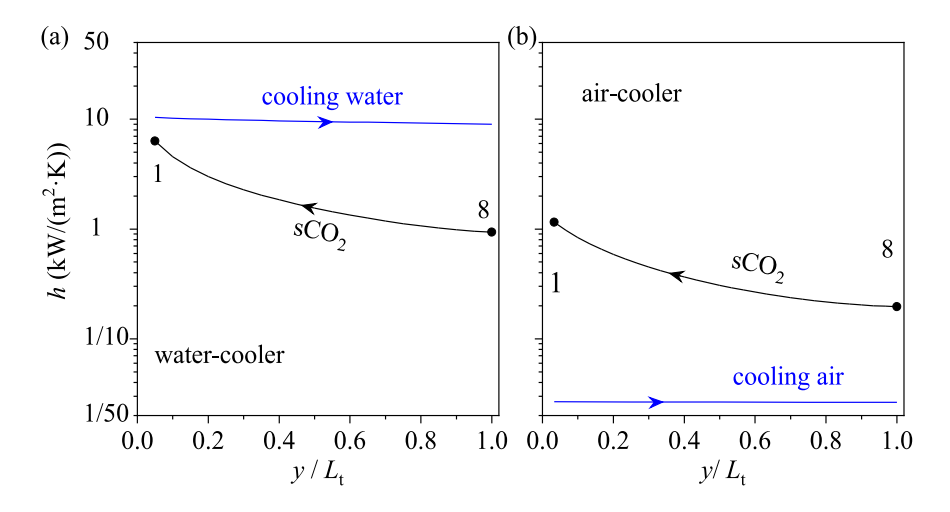


Fig. 12. Heat transfer coefficients between sCO<sub>2</sub> and the cooling fluid of water (a) and air (b).

the four state points during the heat transfer process, and has nothing to do with the heat transfer roadmap. In order to explore the roadmap (integration) effect, the previously proposed integrated average temperature difference (IATD) is applied [64], which is written as follows for the present problem:

IATD = 
$$\frac{\int_{0}^{\Delta H} \left(T_{\text{SCO}_{2}} - T_{\text{cooling fluid}}\right) d(\Delta H)}{\Delta H}$$
(46)

Noting that  $\Delta H$  is the total thermal load during the heat transfer process, the subscript "cooling fluid" refers to either water or air. Giving the T- $\Delta H$  curves shown in Fig. 11, the IATD is 32.7 °C for water cooling and 45.3 °C for air cooling. An important index of IATD is that IATD can characterize the degree of the exergy loss during the heat transfer process.

In the paper, the exergy is only physical exergy, expressed as follows [54]:

$$e = (h - T_0 s) - (h_0 - T_0 s_0)$$
(47)

$$E_{D,\text{water-cooler}} = m_{\text{CO2}}(e_8 - e_1) - m_{\text{w}}(e_{\text{w,o}} - e_{\text{w,i}})$$
 (48)

$$E_{D,air-cooler} = m_{CO2}(e_8 - e_1) - m_a(e_{a,o} - e_{a,i})$$
(49)

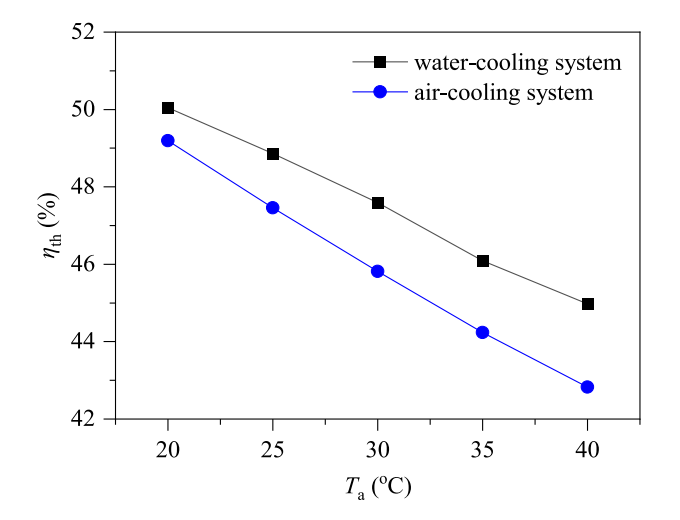


Fig. 13. Thermal efficiencies of the sCO<sub>2</sub> cycle dependent on air temperatures.

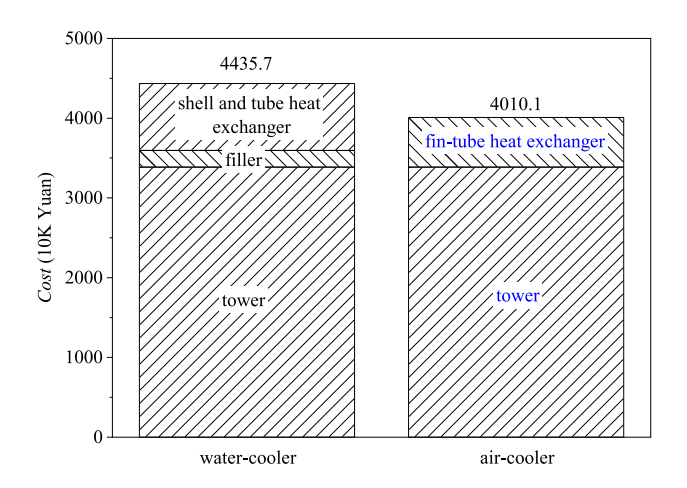


Fig. 14. Comparison of costs for the water-cooler and the air-cooler.

where the subscript 0 refers to the ambient conditions. The exergy loss for air-cooler is 35.1 MW while the exergy loss for water-cooler is 25.4 MW. The larger the IATD, the larger the exergy loss is. The IATD based on Fig. 11 tells us that the air cooling elevates the exergy loss, explaining the cycle efficiency penalty by using the air-cooler instead of the water-cooler. It is noted that the LMTDs have weak difference, but the IATDs are obviously different, regarding the two coolers. The former is related to the heat transfer calculation only, but the later has connection with the exergy loss which is further connected with the cycle efficiency.

We examine the heat transfer coefficients (h) for the sCO<sub>2</sub> and the cooling fluids, noting that  $L_t$  in Fig. 12 represents the total flow length of the heat exchangers. For water cooling, the h is stable along the flow length for water, but increase from the inlet point 8 to the outlet point 1 for sCO<sub>2</sub>. The heat transfer coefficient of sCO<sub>2</sub> reported in this paper is comparable to that in Ref. [40] (see Fig. 7). Giving the logarithm coordinate in the vertical direction, the h of water is apparently larger than those of sCO<sub>2</sub> (see Fig. 12a). The heat transfer coefficients of air are the smallest among the sCO<sub>2</sub> in Fig. 12a–b, water and air (see Fig. 12a and b). The difference of h for sCO<sub>2</sub> in Fig. 12a and b is attributed by the mini temperature difference of sCO<sub>2</sub>, and different flow channel sizes of sCO<sub>2</sub> in the two coolers.

Many works have been done on the water-steam Rankine cycle using the air-cooler and the water-cooler [65], for which the temperature difference between the saturation temperature of water-vapor and the cooling fluids is  $\sim \! 10$  K, which is slightly larger with the air-cooler than that with the water-cooler. However, the mini difference of the temperature differences by using the two coolers creates obvious cycle efficiency penalty. The cycle efficiency is sensitive to the variation of the cooling conditions for the Rankine cycles. This situation is changed for the sCO $_2$  cycle. Due to larger temperature difference of sCO $_2$  and the cooling fluids ( $\sim \! 30$  K LMTD), the cycle efficiency is insensitive to the variation of the cooling conditions, explaining weaker efficiency penalty by using the air-cooler, compared with the Rankine cycle.

As this study focuses on a large-capacity unit with a heat dissipation of approximately 300 MW, a substantial heat exchange area is required. The cooling pipes for air cooling are arranged in parallel, resulting in a minimal pressure drop on the  $sCO_2$  side. In the air cooler, the pressure drop on the  $sCO_2$  side is 8.8 Pa, which is negligible compared to the inlet pressure of 7.6 MPa. On the air side, the pressure drop is 64.4 Pa, which is of the same order of magnitude as reported in Ref. [39]. In the shell-and-tube heat exchanger for the water cooler, the pressure drop on the  $sCO_2$  side is 211.4 Pa, which is also negligible, while the water side experiences a pressure drop of approximately 133.3 Pa. To date, no literature has been found reporting pressure drops on the water or  $sCO_2$  sides in shell-and-tube heat exchangers for  $sCO_2$  cycles, making direct comparisons impossible.

## 3.3. Off-design condition for the air-cooler and the water-cooler

The above section deals with the design condition with the air temperature of  $T_a=20\,^{\circ}\text{C}$ . The effect of  $T_a$  on the cycle efficiency is plotted in Fig. 13, with  $T_a$  varied in the range of  $(20{\sim}40)\,^{\circ}\text{C}$ . It is seen that the efficiencies are always larger for the sCO<sub>2</sub> cycle using the water-cooler than that using the air-cooler. The efficiency gap in between the water-cooling system and the air-cooling system increases with increases of air temperatures. For example, the efficiency gap is 0.8 % at  $T_a=20\,^{\circ}\text{C}$ , but becomes 2.1 % at  $T_a=40\,^{\circ}\text{C}$ . Generally, the increase of  $T_a$  elevates the temperature level of the sCO<sub>2</sub> cycle, deteriorating the cooling effect to weaken the cycle efficiency. The variation trend shown in Fig. 13 is caused by the comprehensive effects of  $T_a$  on the system: (1) the physical properties of air are changed as  $T_a$  changes, (2) the temperature difference between the sCO<sub>2</sub> and the air is changed as  $T_a$  changes, (3) the mass transfer induced evaporative effect between the air and the water in the WCT is influenced due to the variations of  $T_a$ .

#### 3.4. Costs of the air-cooler and the water-cooler

Cost is an important factor for construction of a power plant. Here, we focus on the costs of the water-cooler and the air-cooler, which are shown in Fig. 14 for 300 MW power plant. The water-cooler involves the costs of the WCT including an inside filling zone, and an external STHE. Meanwhile, the air-cooler involves the costs of the tower body and inside finned-tube-heat-exchanger units. The outcome is 43.76 million RMB for the water-cooler, and 40.10 million RMB for the air-cooler. The air-cooler induces a 3.66 million RMB reduction in the construction cost compared with the water-cooler. For the two cooling technologies, the tower bodies have similar construction costs. The difference in the total cooler costs lies in the raised cost of the external STHE for the water-cooler (see Fig. 14). Since the focus of this thesis is a large-capacity unit with heat dissipation of approximately 300 MW, a significant heat exchange area is required. Consequently, 10 heat exchangers are necessary, which contributes to the increased cost of the STHE system.

It should be noted that the above conclusion can be extended to other capacity units as well. Since the cooling load of the  $sCO_2$  cycle is proportional to the unit's capacity, the cost of the cooler will similarly scale with the cooling load. Furthermore, for different capacities, the temperature difference between the inlet and outlet of the cooler remains similar, meaning the relative cooling performance of air coolers and

water coolers will be consistent with the observations for the 300 MW unit.

#### 4. Conclusions

Even tough significant works have been done on the water-steam Rankine cycle using the air-cooling technology, less attention has been paid on the  $sCO_2$  cycle using the air-cooling technology. Here, we provide a comparative study on the  $sCO_2$  cycle coupling with the air-cooler and the water-cooler. Major conclusions are as follows:

- The flow and heat transfer correlations cited from the literature form an integrated model to simulate the air-cooler and the water-cooler, which is further coupled with the thermodynamics cycle. Hence, not only the cycle efficiency, but also the costs of the coolers are determined.
- 2. The sCO $_2$  coal fired power plant with a 300 MW capacity has a 0.8 % cycle efficiency penalty by using the air-cooler instead of the water-cooler, at the air temperature of  $T_a=20\,^{\circ}$ C. The efficiency gap between using the two coolers is increased with increases of the air temperatures.
- 3. At  $T_a=20\,^{\circ}\text{C}$ , the LMTD and the IATD are 33.4  $^{\circ}\text{C}$  and 32.7  $^{\circ}\text{C}$  respectively for the water-cooler, which become 34.2  $^{\circ}\text{C}$  and 45.3  $^{\circ}\text{C}$  respectively for the air-cooler. The elevated temperature level of the sCO<sub>2</sub> cycle and the increased exergy loss in the cooler explain the efficiency penalty by using the air-cooler instead of the water-cooler.
- 4. Compared to the water-steam Rankine cycle with  $\sim \! 10 \, \text{K}$  temperature difference in the cooler, the sCO<sub>2</sub> cycle has larger temperature difference in  $\sim \! 30 \, \text{K}$  level for such heat dissipation, resulting in insensitive effect of the cooling conditions on the cycle performance, explaining weaker efficiency penalty by using the air-cooler instead of the water-cooler.
- 5. For the  $sCO_2$  cycle, the air-cooler induces a 3.66 million RMB reduction in the cost compared with the water-cooler. The raised cost of the STHE for the water-cooler accounts for the cheaper construction of the air-cooler than the water-cooler.
- 6. We conclude that it is preferable to use the air-cooler, which is important to save the water resource under dry weather conditions. The air-cooler of sCO<sub>2</sub> cycle induces mini efficiency drop compared with the water-steam cycle, accompanying by a reduced cost of the cooler compared with the water-cooler.

# CRediT authorship contribution statement

**Yaqin Liu:** Writing – original draft, Software, Methodology, Investigation, Formal analysis. **Jinliang Xu:** Writing – review & editing, Methodology, Funding acquisition, Conceptualization. **Tianze Wang:** Writing – review & editing, Validation, Supervision, Methodology.

# **Declaration of competing interest**

We state that the manuscript titled as "Comparative study on supercritical carbon dioxide cycle using air-cooler and water-cooler "by Yaqin Liu, Jinliang Xu, Tianze Wang does not have any conflict of interest including any financial, personal or other relationships with other people or organizations within three years of beginning the submitted work that could inappropriately influence, or be perceived to influence, the present work.

## Acknowledgements

This work was supported by the National Natural Science Foundation of China (51821004, 52130608).

# Appendix A. Supplementary data

Supplementary data to this article can be found online at https://doi.org/10.1016/j.energy.2024.134148.

# Nomenclature

a	correction factor area, m <sup>2</sup>
A B	width, m
B <sub>c</sub>	baffle clearance, m
C C	cost factor
c <sub>p</sub>	specific heat capacity, J/(kg K)
C C	cost, RMB
d	diameter, mm
D	equivalent diameter, m
e	specific exergy, kJ/kg
$E_D$	exergy destruction rate, MW
f	friction coefficient
$F_{T}$	correction factor
$Fr_D$	correction factor
G	mass flux, kg/(m <sup>2</sup> ·s)
h	heat transfer coefficient, W/(m <sup>2</sup> ·K)
$h_d$	mass transfer coefficient, m/s
H	height, m
i	enthalpy per unit mass, kJ/kg
j 1-	heat transfer correction factor
k K	thermal conductivity, W/(m·K) loss coefficient for cooling tower
L L	length, m
m	mass flow rate, kg/s
Me	Merkel number
n	number
Nu	Nusselt number
P	pressure, MPa
Q	thermal load, MW
R	pressure drop correction factor
Re	Reynolds number
RH	relative humidity
S	entropy per unit mass, kJ/(kg K)
S	entropy, kJ/K
T UA	temperature, K or <sup>o</sup> C overall heat transfer coefficient, W/K
V	velocity, m/s
V	volume, m <sup>3</sup>
W	humidity ratio, kg/kg of dry air
W	work, MW
x	split ratio from the total mass flow rate
Greek symbols	
α	convective heat transfer coefficient, W/(m <sup>2</sup> ·K)
$\alpha_{\mathrm{e}}$	correction factor
δ	thickness, m
ΔL	the length of the node, m
ΔP	pressure drop, MPa
ΔT ε	temperature difference, °C restriction resistance coefficient
η	efficiency
θ	angle, o
λ	diffusion coefficient, m <sup>2</sup> /s
μ	dynamic viscosity, Pa s
ρ	density, kg/m <sup>3</sup>
ξ	correction factor
Subscripts	
a	air
ave	average value
b	tube bundle
bc c	baffle spacing cooler
cr	cross flow section
ct	cooling tower inlet
cte	cooling tower expansion
ctc	cooling tower contraction
d	water droplet
de	drift eliminator
f	fin
fi	filler
fr	frontal
fs	filler support
h	heat source
	(continued on next page)

(continued on next page)

#### (continued)

he	heat exchangers
id	ideal
il	inlet louver
i	inner or inlet
i	calculation node
0	outer or outlet
1	longitudinal tube pitch
ma	moist air
masw	saturated moist air
pc	pseudocritical
pf	fin spacing
pl pl	longitudinal tube
•	transverse tube
pt r	tube row
rz	rain zone
S S	sCO <sub>2</sub>
-	2
sp t	spray zone
*	tube
tcc	effective tube rows crossed in one crossflow section effective tube rows crossed in the baffle window
tcw	
th	thermal
tp	tube pitch
to	cooling tower outlet
ts	tower support
W	water
wp	tube passes
y,z	calculation node
4.5	Abbreviations
AP	air preheater
C	compressor
EAP	external air preheater
HRH	high temperature reheater in boiler
HTR	high temperature recuperator
IATD	integrated average temperature difference
LMTD	logarithmic mean temperature difference
LRH	low temperature reheater in boiler
LTR	low temperature regenerative heat exchanger
RH	reheater in boiler
SH	superheater in upper furnace
T	turbine
TEMA	Tubular Exchanger Manufacturers Association

# Data availability

Data will be made available on request.

#### References

- [1] Wu G, Zeng M, Peng LL, Liu XM, Bo Li, Duan JH. China's new energy development: status, constraints and reforms. Renew Sustain Energy Rev 2016;53:885–96.
- [2] Wang JX, Chen LD, Tan ZF, Du ES, Liu N, Ma J, et al. Inherent spatiotemporal uncertainty of renewable power in China. Nat Commun 2023;14(1):5379.
- [3] Yang YP, Li CZ, Wang NL, Yang ZP. Progress and prospects of innovative coal-fired power plants within the energy internet. Glob Energy Interconnect 2019;2:160–79.
- [4] Brunner C, Deac G, Braun S, Zophel C. The future need for flexibility and the impact of fluctuating renewable power generation. Renew Energy 2020;149: 1314–24.
- [5] Guo JQ, Li MJ, He YL, Jiang T, Ma T, Xu JL, et al. A systematic review of supercritical carbon dioxide (S-CO<sub>2</sub>) power cycle for energy industries: technologies, key issues, and potential prospects. Energy Convers Manag 2022: 115437.
- [6] Holcomb GR, Carney C, Dogan ON. Oxidation of alloys for energy applications in supercritical CO<sub>2</sub> and H<sub>2</sub>O. Corrosion Sci 2016;109:22–35.
- [7] Ma Z, Turchi CS. Advanced supercritical carbon dioxide power cycle configurations for use in concentrating solar power systems. In: Proceedings of the supercritical CO<sub>2</sub> power cycle symposium, session title: supercritical CO<sub>2</sub> power cycle system concepts; 2011. paper number 1, 2011, May 24-25, Boulder, Colorado, USA.
- [8] Iverson BD, Conboy TM, Pasch JJ, Kruizenga AM. Supercritical CO<sub>2</sub> Brayton cycles for solar-thermal energy. Appl Energy 2013;111:957–70.
- [9] Ahn Y, Bae SJ, Kim M, Cho SK, Baik S, Lee JI, Cha JE. Review of supercritical CO<sub>2</sub> power cycle technology and current status of research and development. J Nucl Eng Technol 2015;47(6):647–61.
- [10] Wang CY, Qiao YQ, Liu M, Zhao YL, Yan JJ. Enhancing peak shaving capability by optimizing reheat-steam temperature control of a double-reheat boiler. Appl Energy 2020;260:114341.

- [11] Wang CY, Liu ZF, Fan MY, Zhao YL, Liu M, Yan JJ. Enhancing the flexibility and efficiency of a double-reheat coal-fired power unit by optimizing the steam temperature control: from simulation to application. Appl Therm Eng 2022;217: 119240.
- [12] Li HZ, Zhang YF, Bai WG, Yang Yu, Li KL, Gao W, et al. Control strategies and dynamic experimental tests on the wide-range and rapid load regulation of a first pilot multi-megawatts fossilfired supercritical CO<sub>2</sub> power system. Energy Convers Manag 2023;279:116748.
- [13] Ma T, Li MJ, Xue XD, Guo JQ, Wang WQ, Jiang T. Study of peak-load regulation characteristics of a 1000 MWe S-CO<sub>2</sub> coal-fired power plant and a comprehensive evaluation method for dynamic performance. Appl Therm Eng 2023;221:119892.
- [14] Liese E, Albright J, Zitney SA. Startup, shutdown, and load-following simulations of a 10 MWe supercritical CO<sub>2</sub> recompression closed Brayton cycle. Appl Energy 2020;277:115628.
- [15] Crespi F, Gavagnin G, Sanchez D, Martínez GS. Supercritical carbon dioxide cycles for power generation: a review. Appl Energy 2017;195:152–83.
- [16] Xu JL, Liu C, Sun EH, Xie J, Li MJ, Yang YP, et al. Perspective of S-CO<sub>2</sub> power cycles. Energy 2019;186:115831.
- [17] White MT, Bianchi G, Chai L, Tassou SA, Sayma AI. Review of supercritical CO<sub>2</sub> technologies and systems for power generation. Appl Therm Eng 2021;185: 116447.
- [18] Liu YP, Wang Y, Huang DG. Supercritical CO<sub>2</sub> Brayton cycle: a state-of-the-art review. Energy 2019;189:115900.
- [19] Zhou T, Liu ZX, Li XJ, Zhao M, Zhao YJ. Thermodynamic design space data-mining and multi-objective optimization of SCO<sub>2</sub> Brayton cycles. Energy Convers Manag 2021;249:114844.
- [20] Sanchez Villafana ED, Vargas Machuca Bueno JP. Thermoeconomic and environmental analysis and optimization of the supercritical CO<sub>2</sub> cycle integration in a simple cycle power plant. Appl Therm Eng 2019;152:1–12.
- [21] Park JH, Park HS, Kwon JG, Kim TH, Kim MH. Optimization and thermodynamic analysis of supercritical CO<sub>2</sub> Brayton recompression cycle for various small modular reactors. Energy 2018;160:520–35.
- [22] Tsuzuki N, Kato Y, Ishiduka T. High performance printed circuit heat exchanger. Appl Therm Eng 2007;27(10):1702–7.
- [23] Cho J, Shin H, Cho J, Ra HS, Roh C, Lee B, et al. Preliminary power generating operation of the supercritical carbon dioxide power cycle experimental test loop.

- In: The 6th international supercritical CO<sub>2</sub> power cycles symposium; march 27-29; 2018. Pennsylvania, USA.
- Wright SA, Radel RF, Vernon ME, Rochau GE, Pickard PS. Operation and analysis of a supercritical CO<sub>2</sub> Brayton cycle. Albuquerque: Sandia National Laboratories; 2010. SAND2010-0171.
- [25] Fleming DD, Holschuh TV, Conboy TM, Rochau G, Fuller R. Scaling considerations for a multi-megawatt class supercritical CO<sub>2</sub> brayton cycle and commercialization. ASME 2012:5:953-60.
- [26] Kim DE, Kim MH, Cha JE, Kim SO. Numerical investigation on thermal-hydraulic performance of new printed circuit heat exchanger model. Nucl Eng Des 2008;238 12):3269-76.
- [27] Liu GX, Huang YP, Wang JF, Liu RL. A review on the thermal-hydraulic performance and optimisation of printed circuit heat exchangers for supercritical CO<sub>2</sub> in advanced nuclear power systems. Renew Sustain Energy Rev 2020;133:
- [28] Yang JZ, Yang Z, Duan YY. A review on integrated design and off-design operation of solar power tower system with S-CO2 Brayton cycle. Energy 2022;246:123348.
- [29] Sun E, Xu J, Hu H, Li M, Miao Z, Yang Y, et al. Overlap energy utilization reaches maximum efficiency for S-CO2 coal fired power plant: a new principle. Energ Convers Manage 2019;195:99-113.
- [30] Liu C, Xu J, Li M, Wang Z, Xu Z, Xie J. Scale law of sCO2 coal fired power plants regarding system performance dependent on power capacities. Energ Convers Manage 2020:226:113505.
- [31] Zhu BG, Xu JL, Yan CS, Xie J. The general supercritical heat transfer correlation for vertical up-flow tubes: K number correlation. Int J Heat Mass Tran 2020;148:
- [32] Chen LY, Xu JL, Cao WX, Zhou KP, Liu GL. Supercritical carbon dioxide heat transfer in horizontal tube based on the Froude number analysis. Energy 2024;294:
- [33] Li XY, Qin Z, Dong KY, Wang LT, Lin ZM. Experimental study of the startup of a supercritical CO<sub>2</sub> recompression power system. Energy 2023;284:128538.
- [34] Zhang YQ, Li J, Li ZG, Xin Yan. Numerical comparison of leakage flow and rotordynamic characteristics for two types of labyrinth seals with baffles. J Eng Gas Turbines Power-Trans ASME 2020;142(9):091008.
- [35] Li HZ, Zhang YF, Yao MY, Yang Y, Han WL, Bai WG. Design assessment of a 5 MW fossil-fired supercritical CO<sub>2</sub> power cycle pilot loop. Energy 2019;174:792-804.
- Duniam S, Jahn I, Hooman K, Lu Y, Veeraragavan A. Comparison of direct and indirect natural draft dry cooling tower cooling of the sCO2 Brayton cycle for concentrated solar power plants. Appl Therm Eng 2018;130:1070–80.
- [37] Kroger DG. Air-cooled heat exchangers and cooling towers. PennWell Books; 2004.
- [38] Ehsan MM, Guan ZQ, Klimenko AY, Wang XR. Design and comparison of direct and indirect cooling system for 25 MW solar power plant operated with supercritical CO<sub>2</sub> cycle. Energy Convers Manag 2018;168:611–28.
- [39] Ehsan MM, Wang XR, Guan ZO, Klimenko AY, Design and performance study of dry cooling system for 25 MW solar power plant operated with supercritical  ${
  m CO}_2$ cycle. Int J Therm Sci 2018;132:398-410.
- Wang XR, Li XX, Li OB, Liu L, Liu C, Performance of a solar thermal power plant with direct air-cooled supercritical carbon dioxide Brayton cycle under off-design conditions. Appl Energy 2020;261:114359.
- [41] Khatoon S, Ishaque S, Kim M-H. Modeling and analysis of air-cooled heat exchanger integrated with supercritical carbon dioxide recompression Brayton cycle. Energy Convers Manag 2021;232:113895.
- [42] Deshmukh, A, Kapat, J, Khadse, A. Transient thermodynamic modeling of air cooler in supercritical  $CO_2$  brayton cycle for solar molten salt application. ASME Paper No. GT2019-91409.

- [43] Xie AJ, An LM, Chen H, Xue XJ, Xu G. Performance optimization of the air-cooling system in a coal-fired power unit based on intelligent algorithms. Appl Therm Eng 2023:230:120791.
- [44] Pattanayak L, Padhi BN, Kodamasingh B. Thermal performance assessment of steam surface condenser. Case Stud Therm Eng 2019;14:100484.
- [45] Blanco-Marigorta AM, Victoria Sanchez-Henríquez M, Pena-Quintana JA. Exergetic comparison of two different cooling technologies for the power cycle of a thermal power plant. Energy 2011;36(4):1966-72.
- [46] Yang LJ, Tan H, Du XZ, Yang YP. Thermal-flow characteristics of the new wave finned flat tube bundles in air-cooled condensers. Int J Therm Sci 2012;53:166-74.
- Li L, Du XZ, Yang LJ, Xu Y, Yang YP. Numerical simulation on flow and heat transfer of fin structure in air-cooled heat exchanger. Appl Therm Eng 2013;59:
- [48] Wang XB, Yang LJ, Du Xz Yang YP. Performance improvement of natural draft dry cooling system by water flow distribution under crosswinds. Int J Heat Mass Tran 2017;108:1924-40.
- [49] Chen L, Wang WJ, Kong YQ, Yang LJ, Du XZ. Hot air extraction to improve aerodynamic and heat transfer performances of natural draft dry cooling system. Int J Heat Mass Tran 2020;163:120476.
- [50] Kong YQ, Wang WJ, Huang XW, Yang LJ, Du XZ, Yang YP. Wind leading to improve cooling performance of natural draft air-cooled condenser. Appl Therm Eng 2018:136:63-83.
- [51] Calise F, Libertini L, Vicidomini M. Design and optimization of a novel solar cooling system for combined cycle power plants. J Clean Prod 2017;161:1358–403.
- [52] Xu JL, Sun EH, Li MJ, Liu H, Zhu BG. Key issues and solution strategies for supercritical carbon dioxide coal fired power plant. Energy 2018;157:227-46.
- Bejan A. Advanced engineering thermodynamics. fourth ed. New Jersey: Wiley;
- Chen D. Power cycle analysis. Shanghai Science Press; 1983 [in Chinese]. [54]
- Thulukkanam K. Heat exchanger design handbook. Boca Raton: CRC press; 2013. [55]
- Yoon SH, Kim JH, Hwang YW, Kim MS, Min KD, Kim YC. Heat transfer and pressure drop characteristics during the in-tube cooling process of carbon dioxide in the supercritical region. Int J Refrig 2003;26:857–64.
- [57] Churchill SW. Friction-factor equation spans all fluid-flow regimes. Chem Eng (NY) 1977;84(24):91-2.
- Taal M, Bulatov I, Klemes J, Stehlik P. Cost estimation and energy price forecast for economic evaluation of retrofit projects. Appl Therm Eng 2003;2:1819-35.
- [59] Conradie AE, Buys JD, Kroger DG. Performance optimization of dry-cooling systems for power plants through SQP methods. Appl Therm Eng 1998;18(1-2): 25-45.
- [60] Briggs DE, Young EH, Convection heat transfer and pressure drop of air flowing across triangular pitch banks of finned tubes. Chem Eng Prog Symp Ser 1963;59: 1\_10
- [61] Robinson KK, Briggs DE. Pressure drop of air flowing across triangular pitch banks
- of finned tubes. Chem Eng Prog Symp Ser 1963;62(64):177–83.
  [62] NIST. NIST chemistry WebBook NIST standard reference database number 69. 2022.
- Г631 Wei HM, Huang XW, Chen L, Yang LJ, Du XZ. Performance prediction and costeffectiveness analysis of a novel natural draft hybrid cooling system for power plants. Appl Energy 2020:262:114555.
- Yu C, Xu JL, Sun YS. Transcritical pressure Organic Rankine Cycle (ORC) analysis based on the integrated-average temperature difference in evaporators. Appl Therm Eng 2015;88:2–13.
- [65] Williams CR, Rasul MG. Feasibility of a hybrid cooling system in a thermal power plant. In: Proceedings of the 3rd IASME/WSEAS international conference on energy and environment; 2008. p. 23-5. Cambridge, UK.